VOLUME 18, 1956/57, No. 11 pp. 317-348 Published 9th May 1957

Philips Technical Review

DEALING WITH TECHNICAL PROBLEMS
RELATING TO THE PRODUCTS, PROCESSES AND INVESTIGATIONS OF
THE PHILIPS INDUSTRIES

EDITED BY THE RESEARCH LABORATORY OF N.V. PHILIPS' GLOEILAMPENFABRIEKEN, EINDHOVEN, NETHERLANDS

THE EC 57, A DISC-SEAL MICROWAVE TRIODE WITH L CATHODE

by G. DIEMER, K. RODENHUIS and J. G. van WIJNGAARDEN.

621.385.3.029.6:621.3.032.213.2

The triode is the cornerstone of the still rapidly developing radio industry. Many tubes have been derived from the triode, which itself continues to play an important role. It is a remarkable fact that the triode has also won a place for itself in the new branches of very-high-frequency radio engineering, for which it was at one time thought that only velocity-modulated tubes were suitable. The designers of microwave triodes have, of course, made good use of the latest discoveries. The present article deals, among other things, with the importance in this respect of the introduction of the L cathode.

Introduction

It was at one time thought that the triode, owing to transit-time effects and the low impedances of its inter-electrode capacitances, would not be able to compete in the microwave range with tubes such as magnetrons and klystrons in which transit-time effects are utilized, and travelling-wave tubes, in which, moreover, concentrated capacitances are avoided. Many tube designers have endeavoured, however, to overcome the triode's limitations by still further reducing its dimensions. As a result of combining the work done in different spheres (the manufacture of extremely thin wire for the grids, better cathodes and metal-glass seals, and the refinement of assembly methods), these endeavours have been rewarded with success. For many purposes, triodes are now well able to compete with other tubes in the centimetre wave range, e.g. as oscillators of low power (a few mW), as low-noise wide-band amplifiers and as oscillators and amplifiers of moderate power output (a few watts). The introduction of the L cathode has opened up new perspectives for high-power triodes (20 W or more), the development of which has not yet been concluded.

For certain applications, triodes offer considerable advantages over tubes of the klystron and travelling-wave type. Because of their low supply voltages and the absence of focusing devices, equipment employing triodes can be simplified, reduced in weight and, in many cases, made more cheaply. Moreover, triodes have a large bandwidth, which is an advantage most klystrons lack.

As an example of a microwave triode we shall discuss in this article the type EC 57, which is shown in *fig. 1*. This tube was developed mainly for use in link transmitters, but it can also be put to good use in small, mobile radar units. Up to 4000 Mc/s the tube delivers a power of at least 1.8 W as an amplifier (for 16 Mc/s bandwidth) and 3 W as an oscillator. In designing the EC 57 we have been aided by the insight gained in recent years into the operation of microwave triodes. The L cathode [1]) has also been an important element in the design.

New considerations on the operation of microwave triodes

The operation of triodes at very high frequencies has latterly come to be much better understood.

[1]) H. J. Lemmens, M. J. Jansen and R. Loosjes, Philips tech. Rev. **11**, 341-350, 1949/50.

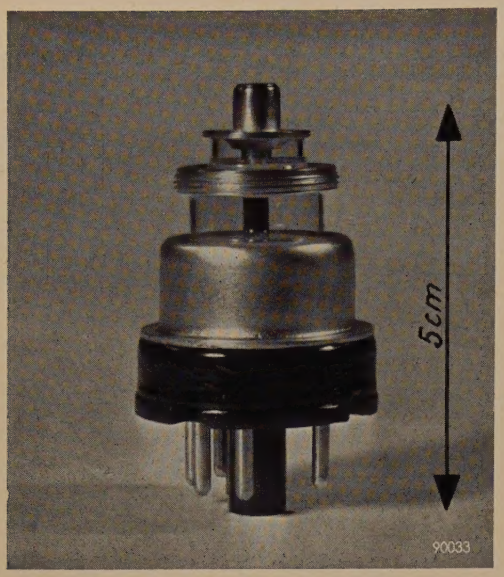

Fig. 1. The microwave triode EC 57.

It was known even before 1940 that, in order to combat transit-time effects, it is necessary not only to make the clearances between the electrodes extremely small but also to use the densest possible electron current. It may be derived that the transit time τ of the electrons travelling from cathode to grid is approximately given by

$$\tau = 6.7\times10^{-10}\left(\frac{d}{j}\right)^{\frac{1}{3}}\text{sec}, \quad \ldots \quad (1)$$

in which d is the distance in cm from cathode to grid and j is the current density in A/cm^2. The favourable influence of a large current density may be broadly understood by the fact that the higher potential needed in the grid plane in order to obtain a denser current gives rise to higher electron velocities and thus to shorter transit times. For a closer derivation of (1) we must consider the potential distribution and the movement of the electrons in the space between the cathode and grid of a planar triode [2]). The triode operates under space-charge conditions, that is to say only some of the electrons emitted by the cathode reach the grid plane. The potential distribution between cathode and grid in this case is set out in *fig. 2* (the grid being represented as the anode of a diode). Near to the cathode there is a minimum in the potential curve. For the derivation of (1) it is assumed that the electrons start in this potential minimum (the quantities d and j being defined accordingly).

[2]) See e.g. G. Diemer and K. S. Knol, Philips tech. Rev. **14**, 153-164, 1952/53.

In reality, the result of a potential distribution as in fig. 2 is that only those electrons that leave the cathode with a sufficiently high initial velocity are able to pass the potential minimum and travel to the grid; the other electrons reverse their direction before the potential minimum and return to the cathode — a subject which will be referred to later.

Another important point affecting the operation of a microwave triode is that the resistance and self-inductance of the supply leads must be kept as low as possible [3]). In particular the self-inductance of the grid lead must be kept low in order to avoid unwanted feedback. These principles have been put into effect in the microwave triodes by making the inter-electrode spacings extremely small and by using disc-seals [4]). The structure of a disc-seal triode is shown diagrammatically in *fig. 3*. The disc-seals form an effective screen between the input and output circuits and may conveniently form part of the wall of a cavity resonator.

The disc-seal triodes described in the book quoted under [4]) were the first triodes to be used at

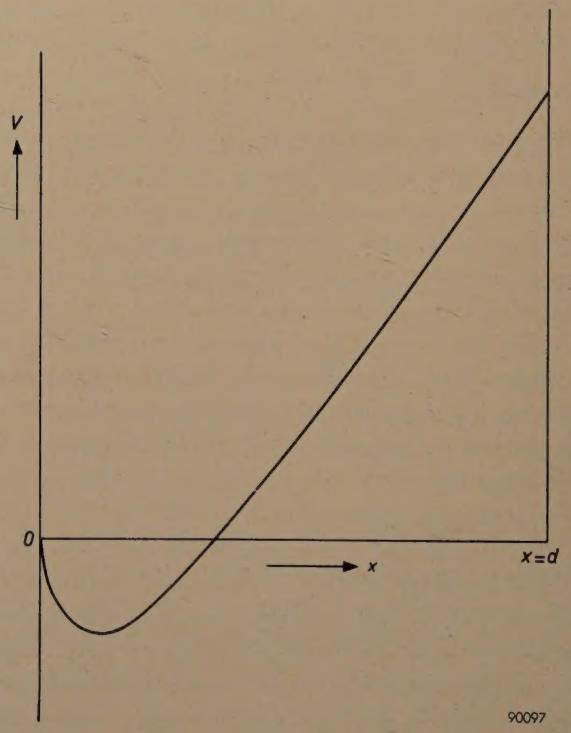

Fig. 2. The potential V as a function of the distance x along the cathode ($x = 0$) — anode ($x = d$) space for a diode operating under space-charge conditions.

[3]) See e.g. M. J. O. Strutt and A. van der Ziel, Philips tech. Rev. **3**, 103-111, 1938; **5**, 172-181 and 357-362, 1940.

[4]) See D. R. Hamilton, J. K. Knipp and J. B. Horner Kuper, Klystrons and microwave triodes, McGraw-Hill, New York 1948, p. 163 et seq.

frequencies from 1000 to 2000 Mc/s. In the EC 57, however, which can be operated up to 4000 Mc/s, another factor of primary importance, apart from the self-inductance, is the resistance of the electrode

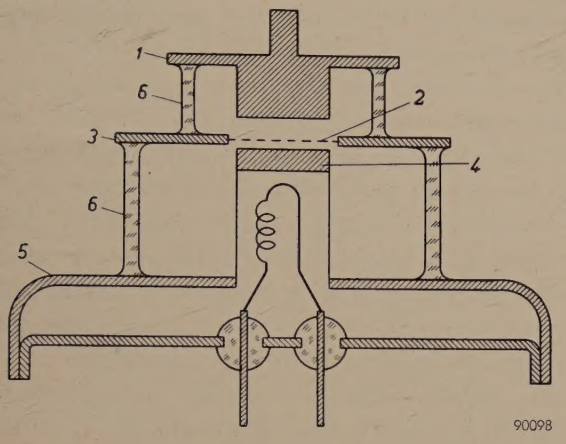

Fig. 3. The structure of a disc-seal triode (schematic); *1* anode disc with anode, *2* grid, *3* grid disc, *4* cathode, *5* cathode disc, *6* glass rings.

leads (i.e. the discs; in the EC 57 of silver-plated chrome-iron). The influence of this series resistance r, which is particularly noticeable at the output side of the tube, may be explained with reference to the circuit in *fig. 4a*. Here, R is the load resistance in which the useful power is dissipated; $g = 1/R$ (see equivalent circuit fig. 4*b*) is the useful load conductance. The resistance r of the leads, which,

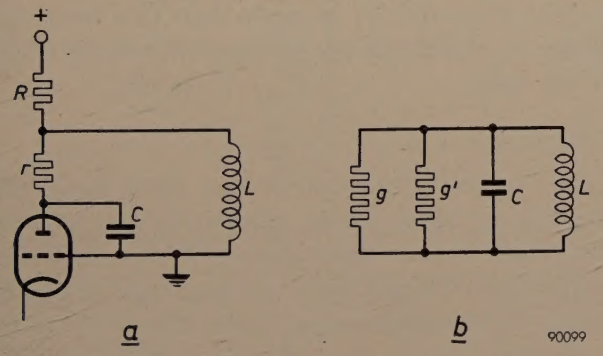

Fig. 4. *a*) Grounded-grid triode circuit, *b*) equivalent circuit.

owing to the skin effect, is proportional to the root of the frequency ω, causes, together with the capacitance C (largely the capacitance of the tube itself) an equivalent parallel conductance

$$g' = \omega^2 C^2 r \propto \omega^{2.5} C^2. \quad . \quad . \quad . \quad . \quad . \quad (2)$$

At 4000 Mc/s the minimum value to which r can be reduced is 0.15 Ω; this is achieved by plating the discs with silver. With this value of r, g' becomes $1/10500\ \Omega^{-1}$. If R is chosen such that the bandwidth is 100 Mc/s, only 17% of the total power delivered by the tube is lost by dissipation in r. (This loss would be much greater in chrome-iron discs without silver plating, r then being 0.75 Ω.)

The effect of further increasing the frequency is a decrease in the gain G (while the bandwidth at optimum matching ($g = g'$) also becomes larger until the value $G = 1$ is reached at the frequency limit). Because of the low value of r and the large ratio of transconductance to capacitance obtained with the L cathode (see below), and also because of efficient dimensioning, the gain of the EC 57 does not begin to drop sharply until about 6000 Mc/s, and the frequency limit is about 15000 Mc/s. As regards dimensioning, for the purpose of obtaining the highest possible frequency limit, the useful electrode surfaces should be made so large that the inter-electrode capacitances have about the same value as the unavoidable capacitances of edges, electrode leads etc. [5]).

There are certain other factors that affect the operation of microwave triodes. It has been found, for example, that the high-frequency currents in the grid wires can themselves give rise to feedback [6]). Moreover, a new type of loss has been discovered, known as total-emission damping [2]) [7]), which is due to the high-frequency energy consumption by the numerous electrons which reverse their direction before the potential minimum and return to the cathode. The effect of this damping is greater the closer the grid is brought to the potential minimum — e.g. by reducing the dimensions. The same electrons also give rise to additional noise, known as total-emission noise.

Differences in transit time profoundly affect the operation of the tube. For instance, even at transit times of several cycles a tube would still have a reasonable amplification provided the transit times of all electrons were the same [8]). It would then be possible to reduce the noise in the output circuit by the use of special circuitry (noise compensation) [9]). The spread in the transit times results in phase differences between the signal currents induced by the various electrons, one consequence of which is reduced amplification. Another important consequence, however, is that the correlation is lost between the different noise currents, and with it the possibility of noise compensation. The spread in

---

[5]) G. Diemer and K. Rodenhuis, Philips Res. Rep. **7**, 36-44, 1952.
[6]) See G. Diemer, Philips Res. Rep. **5**, 423-434, 1950.
[7]) A. van der Ziel and A. Versnel, Philips Res. Rep. **3**, 13-23, 1948.
[8]) A. van der Ziel, Philips Res. Rep. **1**, 381-399, 1946.
[9]) G. Diemer and K. S. Knol, Philips tech. Rev. **14**, 236-244, 1952/53.

transit times has many causes, among which are the finite initial velocity of the electrons, the deviations from the ideal planar triode structure and local variations in work function.

The role of the cathode

In the development of the EC 57 the L cathode was of fundamental importance. Its use resulted in substantial improvements upon microwave triodes with oxide cathodes. One advantage of the L cathode is that, owing to its metallic surface, it gives rise to fewer high-frequency losses than the oxide cathode, the surface of which is a semi-conductor. Furthermore, the L cathode is less susceptible than the oxide cathode to damage from the ion bombardment that arises during the degassing of the anode in the manufacturing stage. (In the disc-seal triode the degassing process cannot be effected by high-frequency heating, as in other tubes, and therefore is performed by electron bombardment from the cathode, which gives rise to a kind of gas discharge between the electrodes.) However, the most important improvements obtained by using the L cathode are based upon the fact that it can tolerate a much higher continuous current density than the oxide cathode although it has a smaller saturation current density. For example, the L cathode can easily yield 0.5 A/cm^2 at a saturation of 2 A/cm^2. The saturation of the oxide cathode is higher, e.g. 10 A/cm^2, but of this only 0.2 A/cm^2 can be utilized if the cathode is to have a reasonable life.

It has already been pointed out that a higher current density is advantageous for reducing electron transit times — and hence also the spread in transit times. The fact that with the L cathode the ratio of anode current to saturation current is much greater than with the oxide cathode has the important consequence of allowing the distance from the cathode to the potential minimum to be reduced to e.g. 6 μ with the given numerical values, as compared with 10 μ in the case of the oxide cathode. The effect of this is to reduce considerably the transit time as well as the number of the electrons that return before the potential minimum. This results in a substantial reduction of the total-emission damping and the total-emission noise.

A further advantage of the higher current density is that a smaller cathode surface is needed for the same transconductance. This means smaller tube capacitances and consequently lower losses in the circuits. Moreover, owing to the correspondingly smaller grid surface, the effect of magnetic feedback through the grid wires is smaller.

Finally, the higher current density of the L cathode as compared with the oxide cathode makes it possible to obtain a higher power output (e.g. 20 W or more) at a given bandwidth. Since the tube described in this article has been developed for moderate power output, we shall not go into this matter here.

Together with the advantages mentioned, the L cathode has certain drawbacks, the effects of which can, however, be compensated by suitable design. The drawbacks referred to are the following:

1) Owing to the higher temperature of the L cathode (1050 °C as against 750 °C for the oxide cathode), the radiation from the cathode makes the grid wires appreciably hotter, so that they are more liable to bend as a result of expansion.
2) The higher heater power calls for special care in the construction of the heater.
3) The more rapid evaporation of barium and barium oxide involves the risk that these materials will form deposits on the grid wires (thereby altering the characteristics of the tube) and on the glass envelope (resulting in additional losses).

The methods that have been adopted to counter these effects, will be discussed below.

Design of the EC 57 triode

We shall consider the components and the assembly of the EC 57 in more detail by reference to *fig. 5*, which shows a simplified cross-section of the tube.

The envelope

The envelope consists of the glass walls (*6*) fused to the chrome-iron components (*1*), (*3*) and (*5*). The latter carry the electrodes and are conveniently termed discs, although their shape is in fact more complicated.

We have already shown that the resistance of the discs must be as small as possible. For this reason the chrome-iron is silver-plated. The grid disc is so designed as to make it impossible for barium evaporating from the cathode to move in a straight line to the glass ring between grid and anode. The barium is thus intercepted at a place where it can do no harm. For the same purpose a shielding ring (*9*) is incorporated which keeps the glass wall between grid and cathode clean.

In some disc-seal triodes the discs are made of copper. Copper being relatively soft, it is then necessary to use ceramic spacers inside the envelope (stacking construction) in order to fix the electrodes

at the required small clearances. The disadvantage of these spacers is that they introduce extra capacitance in the tube. Moreover, because they are usually at a fairly high temperature they give rise to rather large dielectric losses. In the EC 57 using only the chrome-iron discs and glass walls, it proved possible by means of a special method of adjustment (which will be discussed below) to obtain the required grid-cathode separation of 40 μ (and *a fortiori* the much greater grid-anode separation). This considerably reduces the capacitances and the losses.

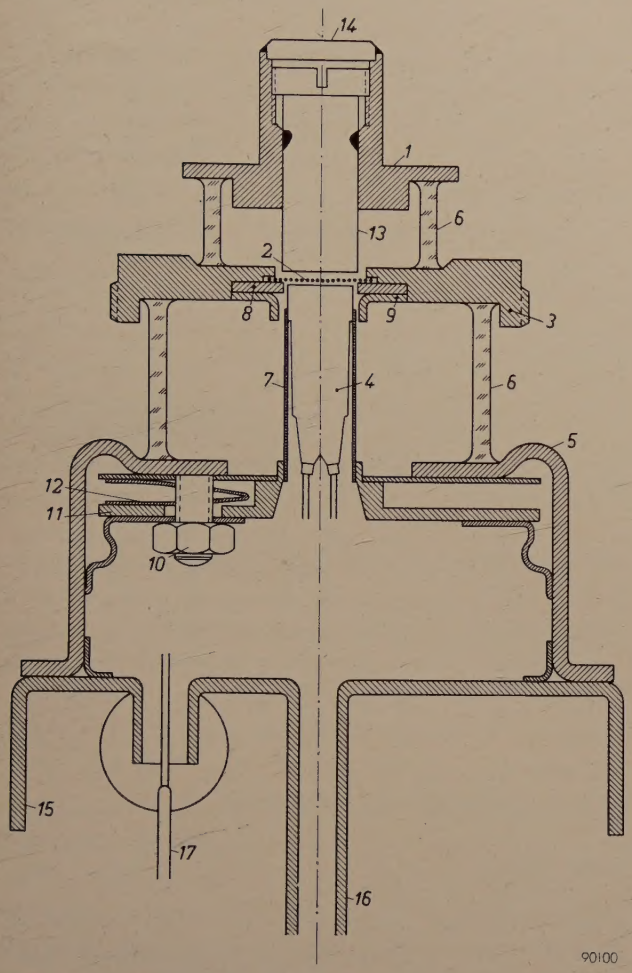

Fig. 5. Simplified section of the EC 57, showing most important parts: *1* anode holder, *2* grid, *3* grid disc, *4* cathode, *5* cathode disc, *6* glass rings, *7* cathode holder, *8* molybdenum frame, *9* shielding ring, *10* nut, *11* cathode base, *12* contact spring, *13* anode, *14* anode cap, *15* base plate, *16* exhaust stem, *17* filament connecting pin.

The cathode

The L cathode (*4*) is fixed to the cathode base (*11*) by means of tantalum foil in tubular form (*7*) (thickness 0.012 mm). Tantalum is easy to work, its heat conductivity is not too high, its electrical conductivity is tolerable and it remains sturdy at the activation temperature of the cathode. The cathode is brought to the appropriate temperature by the heating of a filament, which is sintered in the molybdenum cathode tube with the aid of aluminium oxide, thus ensuring good heat transmission. In this way the temperature of the filament does not become so high as to shorten its useful life.

The grid

Tungsten wire (diameter 7.5 μ) [10]) is used for the grid and is wound on a molybdenum frame (*8*) with a 4 mm square aperture; since the pitch is 48 μ there are more than 80 turns in the frame. *Fig. 6* shows a photograph of this grid enlarged 9 diameters.

During operation the grid wires, as we have seen, become hot as a result of radiation from cathode and anode. In fact, however, a high temperature has a beneficial effect in that it considerably reduces the formation of barium deposits on the grid wires. The thinner the wires the higher their temperature, owing to the diminished heat conductivity to the grid disc. The diameter of the wires is chosen such that, at the temperature in question, the barium evaporates from the wires almost as fast as it arrives from the cathode. If the temperature of the grid wires is too high there is admittedly a great risk of grid emission. In the EC 57, however, this unwanted emission is adequately suppressed by covering the grid wires with a thin layer of gold.

If no precautions were taken the wires would be deformed by expansion. For this reason they are

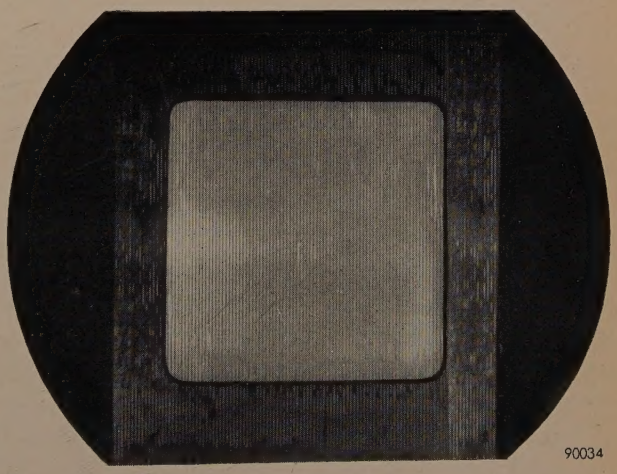

Fig. 6. Photograph of grid enlarged 9×.

[10]) For the manufacture of thin tungsten wire, see: L. Schultink and P. G. van Zanten, Philips tech. Rev. **18**, 222-228, 1956/57.

mechanically pre-stressed. By braking the coil of wire during the winding process, the wire is stressed to about 60% of its tensile strength.

After winding, the turns are gold-soldered to the frame and then removed from one side. The soldering reduces the tensile strain in the grid wires. The reasons for this are many and complicated, the most important being the fact that the molybdenum frame has a somewhat greater coefficient of expansion than the tungsten wires, and that the yield point of the wires is lowered at the soldering temperature (about 1200 °C). A tungsten wire of 100 μ diameter is used as a well-defined wedge and is pressed into the frame perpendicular to the grid wires, on the side free of wires; by this means the frame is made to expand by a precise amount (a few microns), so that the strain returns to the required value. Since the frame aperture is square, the stress in all the wires is increased by the same extent. The tensile stress in the wires is then measured as follows. The grid is placed under a microscope and a flat metal plate is mounted a fraction of a millimetre away, parallel to the grid wires. A high alternating voltage is then applied between grid and plate. At a certain frequency the wires begin to resonate, and the resonance frequency (about 20000 c/s) is related simply to the tensile stress in the wire. In this way it is possible to measure the stress of all wires separately. With tungsten wire of thickness 7.5 μ, the required tensile stress in the wires amounts to about 10 gr per wire. The grid can then tolerate, without deformation, a dissipation of about 1 W, which is amply sufficient for efficient operation.

Assembly of the components

After the grid (*8*) (fig. 5) has been placed in position, the cathode is fitted in the cathode ring (*5*) and temporarily fixed with three nuts (*10*). Between the cathode base (*11*) and the cathode ring there is a 3-lipped molybdenum spring (*12*) which presses the cathode base against the nuts, thus allowing accurate alignment. The distance between grid and cathode is adjusted under a microscope, the optical axis of which coincides with the tube axis, so that it is possible to look through the aperture of the anode holder (*1*). A narrow, parallel beam of light (see *fig. 7*) is obliquely projected on to the cathode: line shadows of the grid wires are then seen on the cathode. By making the shadow of each wire at a given angle of incidence fall exactly under the adjacent wire, the desired spacing can be very accurately adjusted. To ensure that the shadows do not fall under the wrong wires, a capacitance measurement is also carried out, which serves for the rough adjustment. Perfect parallelism is obtained if the shadows over the whole surface lie centrally under the wires. This having been done, the cathode base is fixed by welding.

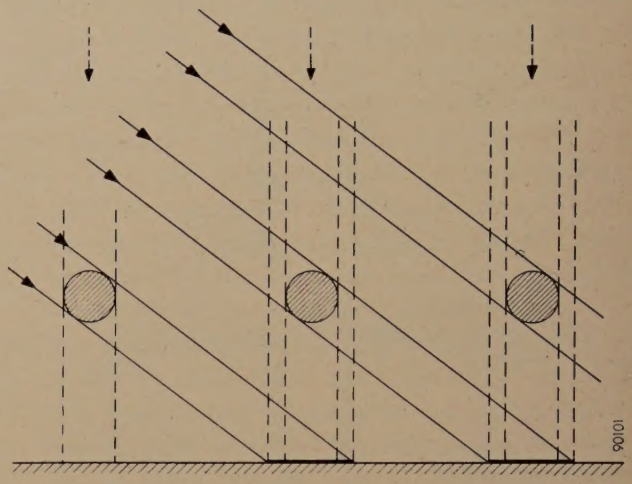

Fig. 7. Precision adjustment of spacing between grid and cathode by shadow method.

The anode (*13*) is then screwed into the anode holder (*1*), and again, by means of a capacitance measurement, adjusted to the correct distance from the grid. The anode cap (*14*) is welded to the anode holder to produce a vacuum-tight seal. Finally, the base plate (*15*) with its exhaust stem (*16*) is welded vacuum-tight to the cathode ring. The tube can now be pumped and outgassed.

Tube data

From the tube data set out in *Table I* it will be seen that two values are given for the capacitances between grid and cathode and between grid and anode, viz.: the static values C_{gk} and C_{ag} and the high-frequency values C_{gk}' and C_{ag}'. The latter values are smaller than the static values owing to the fact that at microwave frequencies only part of the electrode leads acts as a capacitative load.

Table I. Principal data of the EC 57.

Anode voltage	180 V
Anode current	60 mA
Transconductance	20 mA/V
Amplification factor	43
Static grid-cathode capacitance C_{gk}	3.3 pF
H.F. grid-cathode capacitance C_{gk}'	1.8 pF
Static grid-anode capacitance C_{ag}	1.6 pF
H.F. grid-anode capacitance C_{ag}'	0.6 pF
Cathode-anode capacitance C_{ak}	0.04 pF
Life	about 5000 h

The life of the tube is limited mainly by the barium evaporation, in spite of the countermeasures adopted. It has been found, however, that barium evaporation can be appreciably reduced by small modifications in the cathode, so that further improvements in the life of the tube may be expected.

Microwave impedances of the tube

The impedances at microwaves can be calculated with the aid of theoretical considerations based on ideal triodes [11]). Actual triodes differ so much from the ideal that the theory can provide no more than a rough approximation; in practice, the impedances can be determined accurately only by experiment. However, the theory is useful in as much as it shows how the transconductance, for example, depends upon a number of fundamental quantities. Thus, the transconductance at high frequencies is shown to fall only slowly with increasing transit-time angles. The transit-time angle Θ_1 between cathode and grid is, by definition, the average transit time of the electrons over this distance, multiplied by the angular frequency ω of the high-frequency signal. The transit-time angle Θ_2 between grid and anode is defined analogously. The relevant values for the EC 57 at 4000 Mc/s are:

$$\Theta_1 = 3.36 \text{ radians},$$
$$\Theta_2 = 1.46 \text{ radians}.$$

At these values the theoretical transconductance has fallen to 75% of that at low frequency.

The high-frequency input conductance is measured by determining the quality factor at 4000 Mc/s of a cavity resonator mounted between cathode and grid. The grid-anode capacitance in this case must be short-circuited to the high-frequency currents; this can be done by enclosing this capacitance in a second cavity resonator with a resonance frequency differing widely from that of the first. In this way we found a total input conductance of 15 mA/V due to the circuit and the electrons together. By measuring the damping of the cut-off tube, we were able to separate the electronic damping from the other losses (losses in the circuit and in the glass parts of the tube). The latter losses can be represented by a resistance shunted across the grid-cathode capacitance. This resistance amounts to 1700 Ω at 4000 Mc/s, corresponding to a cut-off conductance of 0.6 mA/V, so that the electronic input damping, corresponding to the transconductance, comes to somewhat more than 14 mA/V. This value of the transconductance, which is thus large with respect to the cut-off conductance, is about 30% smaller than the transconductance at low frequency (20 mA/V), in good agreement with the theory. It also appears that there is little influence from total-emission damping in the normal operating region (the above value was measured at an anode current of 30 to 50 mA).

It has already been stated that the cut-off conductance g' of the anode-grid space (equation 2) corresponds to a parallel resistance of 10.5 kΩ, and that this damping appears to have little effect at a bandwidth of 100 Mc/s. At the transit-time angles mentioned, the effect of the electronic output conductance which has a negative value, is also very slight (see [11])).

To investigate the feedback from the output to the input, measurements were made on an amplifier designed for operation with the EC 57 [12]). The change in the input impedance was determined when the anode load was varied. The feedback was found to be caused by:

1) the effect of the anode voltage on the electron current;
2) the capacitance C_{ak};
3) the high-frequency currents flowing in the grid wires [6]).

The feedback depends on the distance between grid and anode, a parameter that can be selected within fairly wide limits. At a certain distance between grid and anode the feedback was reduced to zero. Since, however, the gain at the same bandwidth was found to be higher with slight feedback than without [13]), the grid-anode spacing was adjusted accordingly.

Microwave amplification and noise

For microwave amplification the triode will always be used in a grounded-grid circuit [8])[9]), in which, owing to the high electronic damping of the input circuit, the bandwidth of the amplifier is almost entirely determined by the bandwidth of the output circuit. Neglecting the feedback we may express the product of the power amplification G and the bandwidth B by the following formula [14]),

---

[11]) F. B. Llewellyn and L. C. Peterson, Proc. Inst. Rad. Engrs. **32**, 144-166, 1944.

[12]) This amplifier, the circuitry and coupling elements of which called for special design, will be dealt with in an article shortly to be published in this Review.

[13]) For a discussion of this phenomenon see A. van der Ziel and K. S. Knol, Philips Res. Rep. **4**, 168-178, 1949.

[14]) See e.g. A. H. W. Beck, Thermionic valves, Univ. Press Cambridge 1953, p. 419.

provided the internal resistance of the tube is large with respect to the anode load:

$$GB = \frac{S^2}{2\pi g_i C_{ag}'},$$

where S is the absolute value of the high-frequency transconductance, g_i the total input conductance and C_{ag}' the high-frequency capacitance of the anode circuit, as already defined [14]). Filling in the values determined, we find

$$GB = 3400 \text{ Mc/s}.$$

At a carrier frequency of 4000 Mc/s, values varying between 1500 and 2000 Mc/s have been found in practice. It should be remembered in this respect that constructional limitations may give rise to a somewhat larger capacitance than C_{ag}'.

These remarks apply only to weak signals. At higher power outputs the amplification falls, and in a given amplifier it does so, as may be expected, with the bandwidth remaining almost constant. For example, at a bandwidth of 100 Mc/s the amplification falls 4 dB when the power output is boosted to 1.5 W. In view of the rather low value of the anode load resistance, the power output is mainly limited by the cathode emission.

As an oscillator, the EC 57 at 4000 Mc/s can deliver a power of 3 W with an efficiency of 20%.

The noise factor was measured at various frequencies and was found to be 17 dB at 4000 Mc/s and 16 dB at 3000 Mc/s. At 500 Mc/s it dropped to 5 dB and at 400 Mc/s to 4 dB.

In the development of this microwave triode, important contributions were made by H. J. Lemmens, C. P. Klöpping and C. C. A. M. Moubis. The noise-factor measurements at the lower frequencies were carried out by F. L. H. M. Stumpers.

Summary. A description is given of a disc-seal triode for microwaves, type EC 57, the dimensions and inter-electrode spacings of which are very much smaller than those of normal triodes. Mention is made of various phenomena which were discovered during the use of microwave triodes (e.g. total-emission damping and noise, and a new type of feedback) and which influenced the design of the EC 57. The EC 57 has planar electrodes connected to chrome-iron discs, between which glass rings are fused (disc-seal construction). A major factor in the design is the use of an L cathode, some advantages of which are a high current density and a metal surface, able to withstand the ion bombardment arising during the degassing of the anode. The disadvantage of the relatively heavy evaporation of barium from this cathode is countered by simple measures, which increase the tube's useful life to about 5000 hours. The 7.5 μ thick grid wires are wound, under mechanical pre-stressing, on a square frame. Special techniques have been developed for checking the stress so produced and for adjusting with precision the spacing between grid and cathode. The principal tube data are tabulated and the microwave impedances and feedback are discussed. The product of power amplification and bandwidth is approx. 1600 Mc/s and the noise factor at 4000 Mc/s is 17 dB. As an amplifier the tube can deliver 1.8 W at this frequency, as an oscillator 3 W.

ULTRASONIC MACHINING

I. TECHNIQUE AND EQUIPMENT

by E. A. NEPPIRAS *) and R. D. FOSKETT *).

534.321.9:621.95

The technique of using high frequency mechanical vibrations for machining brittle materials has assumed considerable importance in recent years. In this technique, a resonant electromechanical transducer is used to generate vibrations, at an ultrasonic frequency, which are transmitted to the drilling tool through a mechanical focussing device designed to provide a sufficiently intense vibration at the tool face. The actual cutting agent is an abrasive powder dispersed in a liquid.

The growing interest in this ultrasonic machining technique has made it necessary to obtain an accurate assessment of the potentialities of the method. The first part of this article, printed below, deals with the fundamentals of the technique and gives a description of some ultrasonic drilling machines developed at the Mullard Research Laboratories. The second part of the article, to appear shortly, gives an assessment of the technique in terms of cutting speeds, accuracy and surface finish.

Introduction

The first mention of the possibility of using high frequency electromechanical transducers for machining operations is contained in a paper by Wood and Loomis in 1927 [1]). They showed how, by using a piezo-electric crystal vibrator with a focusing device consisting of a tapered glass tube filled with water, holes could be pierced in a glass plate held against the end of the taper. It was not until the war years (1939-45), however, that the technique was put to a useful purpose, when it was applied on a limited scale for cutting and drilling precious stones. Later it was realized that the principle could be extended and applied to other brittle materials, particularly metals and sintered carbides, some of which were found to be readily machined by this method. In 1948 a patent was published [2]) followed by a number of short articles and notices in the American and British press describing some practical results which had been obtained [3-7]).

The obvious advantage of a reciprocating tool is that the unidirectional motion permits the cavity produced in the workpiece to follow closely the shape of the tool, provided that the tool is restricted to removing particles of material which are small compared with its own dimensions. In practice, this condition can be fulfilled by restricting the motion of the tool so that the chipping occurs on a microscopic scale, at the same time making the cutting process purely an abrasive one, using the tool itself not as a cutting device but merely to hammer particles of abrasive powder into the work. The tool, aided by the abrasive, impresses its image into the work and it is therefore feasible to make cuts of any required shape by giving the tool the appropriate form. Since reciprocating machines are in this respect more versatile instruments than rotary devices, the field of application of this type of drill is very broad: new types of machining operations are possible, many of which had previously not been attempted. Ultrasonic frequencies are more suitable than sonic frequencies for reciprocating drills not only because operation is silent but also from the point of view of cutting speeds (see below).

Fundamentals of the technique

In carrying out a machining operation using the high-frequency reciprocating drill, the tool is pressed into contact with the workpiece using a light pressure superimposed on the alternating motion. An abrasive suspension is fed between the tool and the workpiece. The wearing of the workpiece can be qualitatively explained simply as the result of chipping caused by the abrasive grains being crushed or ground against the work surface by the action of the vibrating tool, the process involving actual contact of the tool with the abrasive particles and the work.

*) Mullard Research Laboratories, Salfords, Surrey, England.

1) R. W. Wood and A. L. Loomis, Phil. Mag. (7) **4**, 417-436, 1927.

2) British Patent No. 602 801, 1948, to Industrial Research Corporation, U.S.A.

3) S. G. Kelley, Materials and Methods **34**, No. 3, Sept. 1951, pp. 92-94.

4) G. H. DeGroat, American Machinist **96**, Sept. 15, 1952, pp. 141-144.

5) R. G. Woold, Machinist **97**, 1601, Sept. 26, 1953.

6) E. A. Neppiras, A high-frequency reciprocating drill, J. sci. Instr. **30**, 72-74, 1953.

7) E. A. Neppiras, Machining by high-frequency vibration techniques, Research (London) **8**, 29-34, 1955.

There are basically two types of operation which can be successfully carried out with reciprocating machines, depending on whether the stock removal is by frictional forces (as in lapping or sizing an existing hole, where the abrasive is rubbed over the surface), or by hammer blows (as in direct piercing or slicing operations). Since in both cases the removal of material is achieved essentially by a chipping action, the technique is limited to comparatively brittle materials and cannot be usefully applied to very soft or merely tough substances. On the other hand, the tool, which is also subject to wear by chipping, is best formed from a tough (not brittle) metal in which the abrasive grains embed themselves without chipping.

The liquid medium holding the abrasive in suspension plays a three-fold role. It acts as a coolant for the tool and workpiece, which would otherwise rapidly become very hot; by capillary action, it allows abrasive to flow to the work area and the worn material to escape; and it achieves a good acoustic bond between the tool and abrasive, allowing an efficient transfer of energy.

Drilling is accompanied by violent cavitation of the liquid between the tool and the work. The audible hiss of cavitation can generally be distinguished above the noise of the actual grinding. The cavitation occurs in the form of streamers of bubbles originating from points on the tool and work. Experiments have shown that the general turbulence produced in the liquid by the motion of these bubble streamers probably helps considerably in stirring up the abrasive mixture under the tool. In this way, by ensuring that broken abrasive is replaced by fresh material and at the same time removing abraded material from the work area, the cavitation action results in an increase in cutting speed. In fact, to a large extent, cutting rates are found to correlate with the observed cavitation intensity.

The cavitation streamers actually consist of multitudes of bubbles in a very violent state of agitation. Bubbles of this sort have an erosive action on solid surfaces and this effect almost certainly accounts for some of the tool wear obtained. The work also often shows wear markings, some of which appear to follow the pattern of the cavitation streamers. They appear to be channels cut into the material merely by the motion of cavitation streamers, carrying abrasive grains with them. The streamers follow fixed paths and the abrasive particles tend to cut comparatively deep furrows in these places. The wear produced in this way is not important from the point of view of stock removal, but it does, of course, affect the quality of the surface finish obtained and when this is an important consideration, these markings must either be removed after formation or prevented from occurring. This can be done by ensuring that the drilling operations are carried out so rapidly that a stable streamer pattern is not allowed to form.

In the majority of the applications of this technique the three considerations of most practical importance are the cutting speeds, surface finish and machining accuracies obtainable. The most important of these, the cutting speed, is to a large extent dependent on the characteristics of the vibrator itself, e.g. vibration amplitude and frequency, and on the static load between tool and work. Before an efficient drilling instrument can be designed, we must know how these factors are related.

Experience shows that cutting rates depend very much on the nature of the oscillatory motion of the tool. A series of drilling tests in glass showed that under many conditions of operation cutting rates are approximately proportional to the square of the oscillatory amplitude. This is shown in *fig. 1*, where the mean penetration rate is plotted against oscillatory amplitude for each of four drills vibrating at different frequencies, the experimental conditions being otherwise identical in all cases. However, experiments have also shown that, for operations which do not involve frictional forces (lapping) but only direct piercing of the material, there is a practical limit to the usable oscillatory amplitudes: little advantage is to be obtained in making the peak-to-peak oscillatory amplitude of the tool very large compared with the grain dimensions of the abrasive [8]). Moreover, whatever abrasive is used, if the impulse per blow is increased, a point is reached where, because of spraying of the abrasive, it becomes impossible to retain the abrasive paste under the tool at sufficient concentration to allow an efficient cutting action to be obtained. Although these restrictions apply only to direct piercing operations, in order to produce a versatile machine tool capable of both piercing and lapping operations a definite limit must be placed on the oscillatory motion of the tool.

Cutting rates increase somewhat less than proportionately with operating frequency, at ultrasonic frequencies, for constant oscillatory amplitude

---

[8]) A recent paper by D. Goetze (J. Acoust. Soc. Amer. **28**, 1033-1037, 1956) on cutting speeds in *tool steel*, shows an approximately linear increase of cutting rates with amplitude. These results, however, refer to peak-to-peak amplitudes up to 0.004″, which are about twice the dimensions of the abrasives used. See also Part II of this article, to appear in the following issue of this Review.

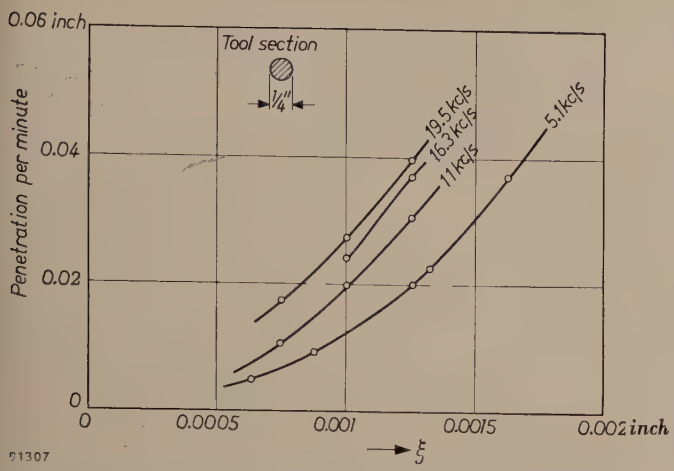

Fig. 1. Cutting rate as a function of oscillatory amplitude ξ (peak-to-peak) for shallow cuts in glass, at four operating frequencies and for constant static load.

and constant static load. In effect this means that the velocity of the tool is of less importance in determining cutting rates than the oscillatory amplitude. The curve shown in *fig. 2* is typical of measured results.

Cutting rates are strongly dependent on the static load imposed between the tool and workpiece and on the tool-face area [9]), and also on the size and nature of the abrasive particles.

These questions will be discussed in greater detail in Part II of this article. At present, we are interested in the light they throw on the requirements to be fulfilled by the drill vibrator. This consists essentially of two parts: a transducer and a velocity transformer.

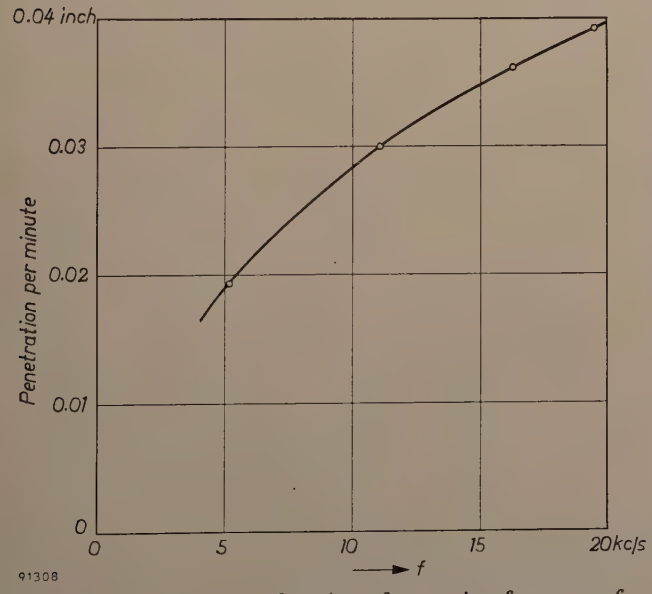

Fig. 2. Cutting rate as a function of operating frequency f, at ultrasonic frequencies, for a peak-to-peak amplitude of 0.00125" and constant static load.

[9]) See A. Nomoto, J. Acoust. Soc. Amer. **26**, 1081-1082, 1954 and also Part II of the present article.

The transducer

The indications are that resonant piezomagnetic[10]) transducers (magnetostrictors) are likely to prove the most valuable of the available types for the present application [11]). Purely from the point of view of power efficiency a low frequency is an advantage, but there are also obvious advantages in keeping the frequency in the ultrasonic range, from the point of view of inaudibility and to keep the vibrator within reasonable limits of size. It is well known that piezomagnetic resonators are more easily constructed as efficient transducers at low ultrasonic frequencies than any other type of electromechanical transducer. Also, in an application of this sort, the transducers must be capable of withstanding long periods of use under ordinary workshop conditions: piezomagnetic metallic materials are robust and not easily damaged either by rough handling or by the rather high temperatures to which they may be subjected in operation. Under specific pre-stressed conditions, certain recently-developed low-porosity piezomagnetic ceramics [12]) (e.g. nickel-cobalt ferrites) and piezoelectric ceramics [13]) (e.g. lead titanate-zirconates), though somewhat less robust, would also be suitable. Other types of electromechanical transducer such as piezoelectric crystals are more fragile and temperature-sensitive.

As the transducer, only longitudinally vibrating piezomagnetic resonators need be considered here. The most economical form is a consolidated laminar stack driven into resonance by passing a current, at the appropriate frequency, through a coil wound round it, the transducer being biased magnetically by the application of a suitable polarizing field: the optimum biasing point is chosen to give maximum magnetomechanical coupling in the transducer material and corresponds to a flux density about 2/3rds of saturation in most piezomagnetic materials. To achieve this flux density and also to provide a path for the alternating flux, it is generally

[10]) The term *piezomagnetism* is used to represent all reversible, nearly linear magnetomechanical phenomena in polarized ferromagnetic materials, to distinguish them from the irreversible, roughly quadratic effects in unpolarized ferromagnetics. The term *magnetostriction* is used quite generally to include both effects. See for example G. Bradfield, Acustica **4**, 171-181, 1954, and the second paper referred to in note [12]).

[11]) For further information on ultrasonic transducers and on ultrasonic techniques generally, see for example, T. F. Hueter and R. H. Bolt, Sonics, Chapman and Hall, London 1955.

[12]) U. Enz, Die Erzeugung von Ultraschall mit Ferriten, Tech. Mitt. P.T.T. **33**, 209-212, 1955. C. M. van der Burgt, Ferroxcube materials for piezomagnetic vibrators, Philips tech. Rev. **18**, 285-298, 1956/57.

[13]) W. P. Mason, J. Acoust. Soc. Amer. **28**, 1207-1218, 1956.

convenient to include a flux return path in the form of a laminated yoke of high permeability, low-loss material. A transducer of this type is shown in the sketch of *fig. 3*.

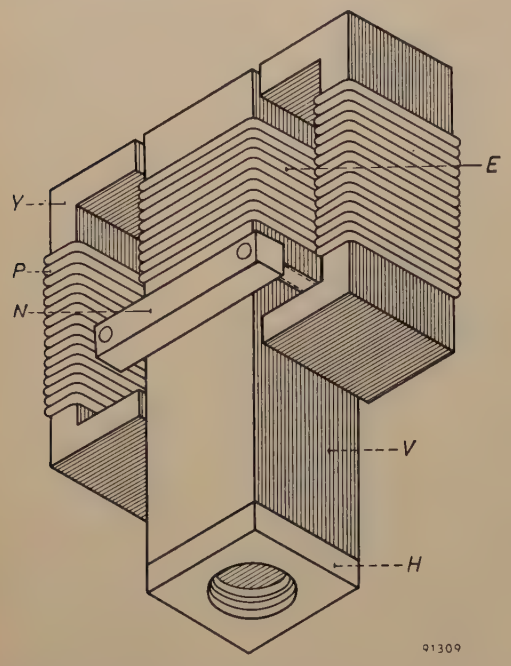

Fig. 3. Essentials of the vibration transducer as used for low-power ultrasonic drills. *Y* laminated yoke, *P* polarizing windings, *N* nodal clamp, *E* energizing coil, *V* laminated vibrating member, *H* tapped steel stub-holder. The vibrating member *V* is $\lambda/2$ in length.

The additional lamination structure complicates the mechanical design of bar-type structures and becomes inconvenient if the transducer is operated at a power level such that water-cooling is necessary. In such cases, a simpler but less efficient alternative is the window type of construction which is also widely used in ultrasonic work. These transducers consist essentially of two laminated bars joined at the ends. The stack is wound toroidally with a single coil which carries both direct polarization and alternating drive currents. A typical window-type transducer used in ultrasonic drills is shown in the photograph of *fig. 4* (see also fig. 9). These transducers are not capable of generating such high vibration intensities as are the bar-type units under comparable conditions of drive [14]). Nevertheless, because of their simple construction and ease of cooling they are generally preferred to bar types in the larger models of ultrasonic machine tools.

[14]) H. H. Rust and E. Bailitis, Kritische Betrachtungen über die linearmagnetostriktive Ultraschall-Erzeugung mittels tonpilzartiger Schwinggebilde, Akust. Beihefte, 1952, No. 2, pp. 89-90.

The practical limit, referred to earlier, to the usable oscillatory amplitudes for machining purposes is too large to be attained at the vibrating face of the free transducer. In the transducer, the limit is set by saturation effects and by the danger of fatiguing the piezomagnetic material under the large alternating stresses set up in it. It is, however, possible to increase the amplitude at the tool by directing the vibrational energy on to it through a mechanical focusing device (velocity transformer). In this way maximum cutting rates can be achieved.

The velocity transformer

The transducer-transformer-tool system which forms the basis of the ultrasonic drill is essentially a resonant mechanical transmission line, two or more half-wavelengths long. The velocity transformer itself generally consists of a tapered metal stub, of suitable high fatigue strength and high mechanical *Q*, which is rigidly bonded to the transducer face. The transformer stubs used in ultrasonic machine tools are generally designed to be resonant at the transducer frequency, as this not only simplifies the design calculations but also allows interchangeable stubs to be used without changing the distribution of nodal planes in the system or its resonant frequency. The importance of this arises from the fact that for the purpose of support it is necessary to provide a rigid clamp, and to avoid excessive damping this should be located at a displacement node; clearly the latter should remain fixed, independent of the stub used and its loading.

The resonant length of tapered metal stubs differs from that for parallel-sided members and depends on the form of the taper and the trans-

Fig. 4. Transducer-transformer-tool system used on the high-power ultrasonic drill (input power 2 kW, frequency $\sim$ 20 kc/s). The slotted ring clamps the final $\lambda/2$ stub to the upper mounting stub.

formation ratio required. Calculations are simplified if the stub section is made to change exponentially. In practice therefore this is often done and the design of stubs of this form has been worked out in some detail (see below and [6])). The increase in vibration amplitude ξ is always exactly equal to the root of the inverse ratio of the end areas for any taper, provided that the maximum lateral dimension of the stub is small in relation to the wavelength. In other words, in any continuous resonant loss-free stub of any number of $\lambda/2$ sections, the product area $\times \xi^2$ is constant at all anti-nodal planes and the transformer provides an increase in vibration intensity only at the cost of a reduction in the effective drive fase area.

The equation giving the motion of a tuned stub of varying section can be obtained by analogy with the acoustic transformer (or acoustic horn) of which the general equation relating the velocity potential φ with distance x along the horn and time t is

$$\frac{1}{c^2}\frac{\partial^2\varphi}{\partial t^2} = \frac{\partial^2\varphi}{\partial x^2} + \frac{\partial\varphi}{\partial x}\cdot\frac{\mathrm{d}}{\mathrm{d}x}\ln A, \quad \ldots \quad (1)$$

where c is the velocity of sound in the medium and A the cross-section at x. Assuming the vibrations to be simply harmonic, we can write $\partial^2\varphi/\partial t^2 = -\omega^2\varphi$, where ω is the angular frequency, and by substitution in equation (1) we eliminate the time variable and obtain

$$\frac{\mathrm{d}^2\varphi}{\mathrm{d}x^2} + \frac{\mathrm{d}\varphi}{\mathrm{d}x}\cdot\frac{\mathrm{d}}{\mathrm{d}x}\ln A + \frac{\omega^2}{c^2}\varphi = 0.$$

This equation, which holds for any law of taper, is true only if the largest diameter of the horn is small compared with the wavelength of the vibrations in it and if the "flare" of the taper is not greater than a critical value. For the particular case of the exponential taper, the solution is simple. Here, if $A = A_0 \exp(-\gamma x)$ where A_0 is the area of the stub at the wide end and the exponent γ defines the flare of the taper,

$$\frac{\mathrm{d}^2\varphi}{\mathrm{d}x^2} - \frac{\gamma\,\mathrm{d}\varphi}{\mathrm{d}x} + \frac{\omega^2}{c^2}\varphi = 0,$$

or, since the particle velocity $v = -\mathrm{d}\varphi/\mathrm{d}x$,

$$\frac{\mathrm{d}^2v}{\mathrm{d}x^2} - \gamma\frac{\mathrm{d}v}{\mathrm{d}x} + \frac{\omega^2}{c^2}v = 0,$$

of which the general solution is

$$v = (K_1\cos\omega x/c' + K_2\sin\omega x/c')\exp(\gamma x/2), \quad \ldots \quad (2)$$

where

$$c' = c/(1-\gamma^2c^2/4\omega^2)^{1/2}. \quad \ldots \quad (3)$$

Thus the effect of the taper is to increase the effective velocity of sound waves in the material by the factor $1/(1-\gamma^2c^2/4\omega^2)^{1/2}$.

It can be seen that the velocity is real only when γ is less than $2\omega/c$: this is the critical value referred to above, for the exponential case. Transmission ceases when the flare becomes greater than this value; the horn is an effective filter and this condition determines the cut-off frequency. A consequence of this increase in the effective velocity of sound is that the length corresponding to the fundamental resonance of a tapered stub of this form is greater than that of a uniform rod and is given by $l = c'\pi/\omega = \lambda'/2$.

The constants K_1 and K_2 in equation (2) are determined from the appropriate boundary conditions. Considering the fundamental resonance, $v = v_0$ at $x = 0$, where v_0 is the velocity of the transducer face, and the strain is zero at the free end where $x = l = c'\pi/\omega$. These conditions give

$$K_1 = v_0 \quad \text{and} \quad K_2 = -\gamma c'v_0/2\omega,$$

so that

$$v = v_0\,[\cos\omega x/c' - (\gamma c'/2\omega)\sin\omega x/c']\exp(\gamma x/2). \quad \ldots \quad (4)$$

For the half-wavelength stub, at $x = l$, the particle velocity $v_1 = -v_0\exp(\gamma l/2)$, so that

$$-v_1/v_0 = (A_0/A_1)^{1/2} = \exp\,\gamma l/2 = a, \text{ say,}$$

where A_1 is the area of the stub at $x = l$. Thus, for a $\lambda/2$ resonant stub the particle velocities, and therefore amplitudes, are increased at the small end, as compared with the large end, in the ratio of the square root of the inverse area ratio.

The quantity a mentioned above is a useful design parameter. The effective velocity of the sound waves may be conveniently expressed in terms of the ratio a of the particle velocities at the small and large ends. Since $\gamma = (2/l)\ln a$ and $c' = \omega l/\pi$, equation (3) may be re-written as

$$c' = c/[1-(c/c')^2(\ln a)^2/\pi^2]^{1/2},$$

which rearranged gives

$$\frac{c'}{c} = \sqrt{1+\left(\frac{\ln a}{\pi}\right)^2}. \quad \ldots \quad (5)$$

The distance x_n from the large end to the displacement node may also be expressed in terms of a. From (4), the particle velocity is zero at the point x_n given by

$$\cot\frac{\omega x_n}{c'} = \frac{\gamma c'}{2\omega} = \frac{\ln a}{\pi}, \quad \ldots \quad (6)$$

and since this is positive, $x_n < \lambda'/4$.

The plane of maximum particle velocity is found by differentiating (4) with respect to x and equating to zero:

$$\frac{\partial v}{\partial x} = v_0\frac{\gamma}{2}\exp\left(\frac{\gamma x}{2}\right)\left[-\left(\frac{\gamma c'}{2\omega}+\frac{2\omega}{\gamma c'}\right)\sin\frac{\omega x}{c'}\right]. \quad \ldots \quad (7)$$

This is zero for $x = 0$ and $x = \lambda'/2 = l$. The planes of maximum particle velocity are therefore at the extremities.

The strain $\varepsilon(x)$ in the exponential stub is proportional to (7), since $\varepsilon = \partial\xi/\partial x$ which is proportional to $\partial v/\partial x$. Also, for the stress distribution $\sigma(x)$ we have

$$\sigma(x) = E\varepsilon(x) = E\frac{\partial\xi}{\partial x} = K\,v_0\exp\left(\frac{\gamma x}{2}\right)\sin\frac{\omega x}{c'}, \quad \ldots \quad (8)$$

where K is a constant involving γ, c', ω and the Young's modulus E. Differentiating with respect to x and equating to zero we get

$$\frac{\partial\sigma(x)}{\partial x} = K\,v_0\frac{\omega}{c'}\exp\left(\frac{\gamma x}{2}\right)\left[\frac{\gamma c'}{2\omega}\sin\frac{\omega x}{c'} + \cos\frac{\omega x}{c'}\right] = 0,$$

or, since $\gamma c'/2\omega = (\ln a)/\pi$,

$$\cot\frac{\omega x_\sigma}{c'} = -\frac{\ln a}{\pi}, \quad \ldots \quad (9)$$

which gives the position of maximum stress x_σ in the exponential stub. The negative value of $\cot\omega x_\sigma/c'$ implies that $x_\sigma > \lambda'/4$, and comparing (9) with (6) we see that x_σ and x_n are in fact equidistant from the mid-point of the stub (see fig. 5).

The required drilling tool may be screwed or brazed to the end of the stub, the stub generally being chosen so that the dimensions of its free end

are comparable with the tool size. Consequently, to accommodate a large range of tool sizes it is convenient to provide a range of matching transformers having different transformation ratios and therefore different end diameters. Typical transformer stubs are shown in *fig. 5* with drilling tools attached.

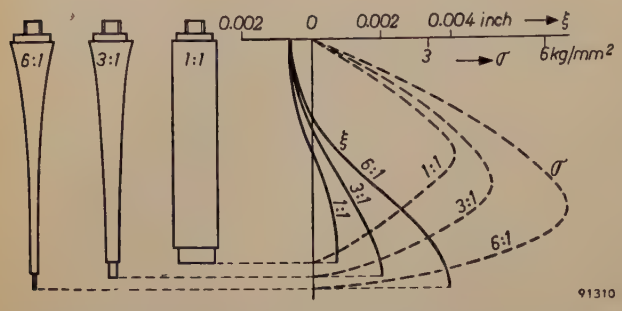

Fig. 5. Half-wavelength velocity transformer stubs with tools attached, showing corresponding amplitude and stress distributions (measured).

A considerable increase in efficiency can be obtained, and the product $A\xi^2$ at the work-face can be greatly increased, by employing multiple massive coupling stubs and transformers, in which an area discontinuity exists at (displacement) anti-nodal junctions (*fig. 6*). In this way the distribution of vibrational energy in the whole system is re-arranged in such a way that a bigger fraction of the total energy is stored in the less lossy parts, i.e. in the velocity transformer(s). The efficiency of such arrangements depends on the stubs remaining very

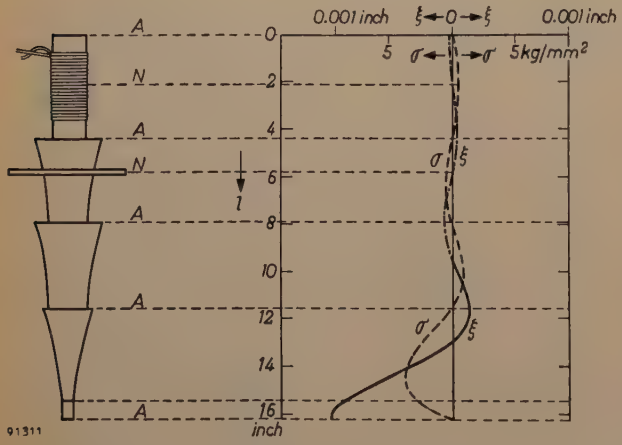

Fig. 6. Transducer-transformer system with step discontinuities at antinodal junctions, showing amplitude and stress distribution (measured). Displacement nodes and antinodes are indicated by *N* and *A* respectively.

nearly resonant under all practical loading conditions (so that the stress transmission across the area discontinuity is small). The mechanical Q of the unloaded system increases and the magnetomechanical coupling coefficient [15]) $\bar{k}$ is reduced in such a way that the product $|\bar{k}|^2Q$ remains approximately constant. Because of its constancy over a wide range of conditions this product is a very valuable design parameter. When resonant matching stubs are used, the product $A\xi^2$ referred to the transducer face is proportional to $(|\bar{k}|^2Q)^2$ for constant driving conditions if the stubs can be assumed loss-free. If not, then this product decreases with increase in mass of the coupling stubs, being very nearly inversely proportional to the total mechanical damping of the system. In practical cases, therefore, there is of course a limit to the vibration intensity obtainable at the working face under free-running conditions, but this will be very high when the stubs are of low-loss material, corresponding to a high mechanical Q of the system.

Two other measures may be mentoined by which, under certain conditions, drilling efficiency may be increased above that obtainable with simple continuous stubs.

1) Useful practical mechanical transforming systems can be designed having discontinuities of area in planes other than the displacement antinodes. In particular, a $\lambda/2$ stub consisting of two $\lambda/4$ cylindrical sections of different areas (see fig. 9) gives an amplitude transformation in the inverse ratio of the end areas (i.e. a greater ratio than the corresponding smoothly-tapered transformer). However, the alternating stress developed in a transformer of this sort is greater than for tapered stubs giving the same drive face amplitude, so that mechanical fatigue troubles may be encountered. The use of these double quarter-wave stubs is therefore restricted to transforming comparatively small end-face amplitudes.

2) As mentioned above, matching stubs must generally be chosen so that the end dimensions are comparable with the tool size. Also a tool loading somewhat below optimum is normally used, in order that small changes in tool face area and loading conditions do not cause too severe mismatching of the amplifier. It is sometimes possible to go some way towards increasing drilling efficiency, however, (without the necessity of increasing the unloaded Q of the system) by merely increasing the cutting area of the tool in relation to the transformer end area. (In order to take advantage of this, however, the whole electromechanical system has to be designed for one given operation.) In this way the radiation loading due to the liquid medium and the work loading are both increased directly. If the tool area is considerable the radiation loss from the free part of the upper surface may be eliminated by providing acoustic pressure-release material (sponge rubber or a similar material) on this surface.

When using this arrangement it is important to ensure that the dimensions of the tool (its thickness especially) are such that no severe flexural modes can be excited.

---

[15]) For the definition of the *material* constant k, see for example the paper by C. M. van der Burgt mentioned in note [12]). Apart from this k, other coupling coefficients may be defined which also take into account the nature and dimensions of the vibrating system, viz. $k_{y/2}$ (for a $\lambda/2$ resonator), $k_{y/2,\,\mathrm{metal}}$ (for a $\lambda/2$ laminated metal resonator, $< k_{y/2}$, owing to eddy current losses) and an *overall* coupling coefficient $\bar{k}$ (for a composite system, e.g. resonant transducer + resonant transformer(s) + tool). It is this last, $\bar{k}$, with which we are concerned here.

Ultrasonic drills

As examples of the application of the design principles outlined above, two ultrasonic machining instruments developed and produced by the Mullard Research Laboratories will be described — a small instrument capable of small-scale drilling work which uses a laminated bar-type transducer, and a full-sized machine tool for general workshop use which uses a laminated window-type transducer. The smaller instrument is operated at an input power level sufficiently low that external cooling of the transducer is not needed, while in the larger machine it is necessary to water-cool the transducer. Most of the drilling work described in this paper was carried out with one or other of these machines.

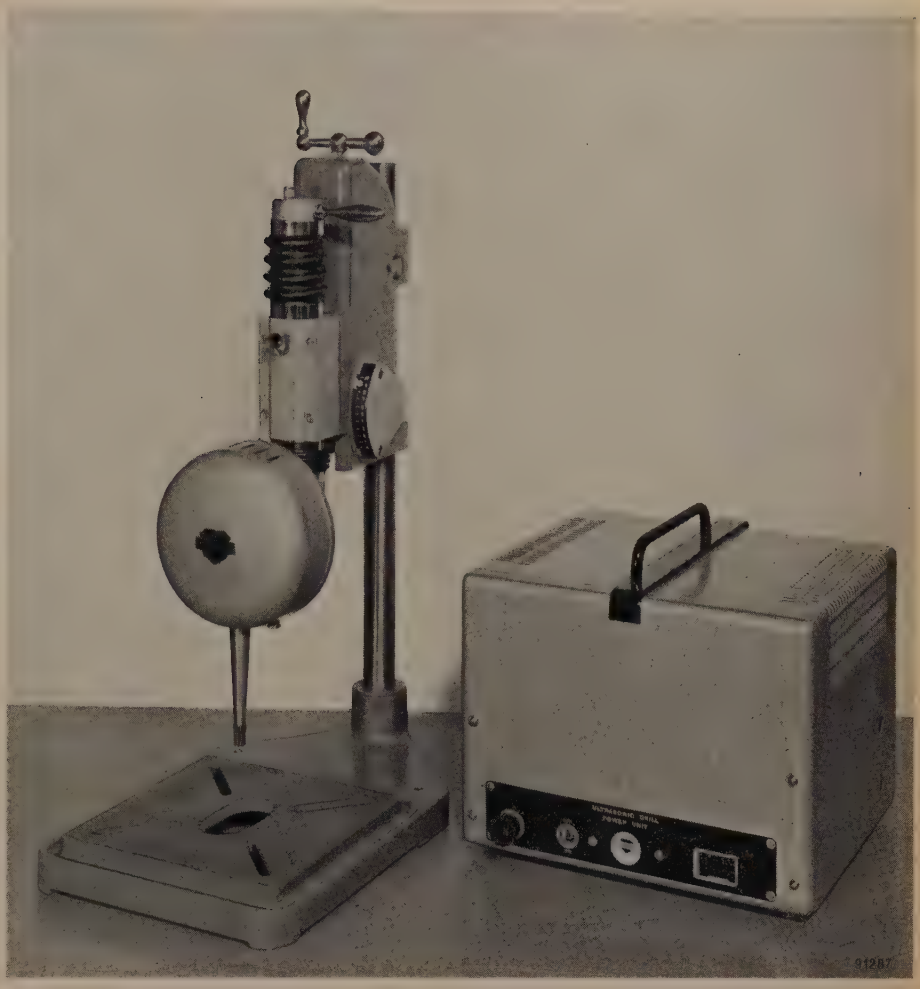

Fig. 7. Low-power ultrasonic drill (input power 50 W, frequency ~20 kc/s; Mullard type E 7682).

The low-power drill is illustrated in *fig. 7*. This drill is fed from an oscillator supplying 50 W at about 20 kc/s. The transducer (fig. 3) consists of a $\frac{3}{4}$ inch square stack of laminations of nickel which have been given suitable magnetic properties by an appropriate heat treatment. The laminations are bonded together by an insulating cement and fixed to the lower end of the stack is a steel-bush which is tapped to serve as a holder to accommodate a range of velocity transformers. The vibrating member is clamped rigidly at its centre (which is a node) and its upper half is surrounded by the energizing coil wound on a former which, to avoid mechanical damping, does not make physical contact with the vibrating laminations. To drive the transducer a conventional oscillator and power amplifier combination is used. A block diagram of the set-up is shown in *fig. 8*. The output from the

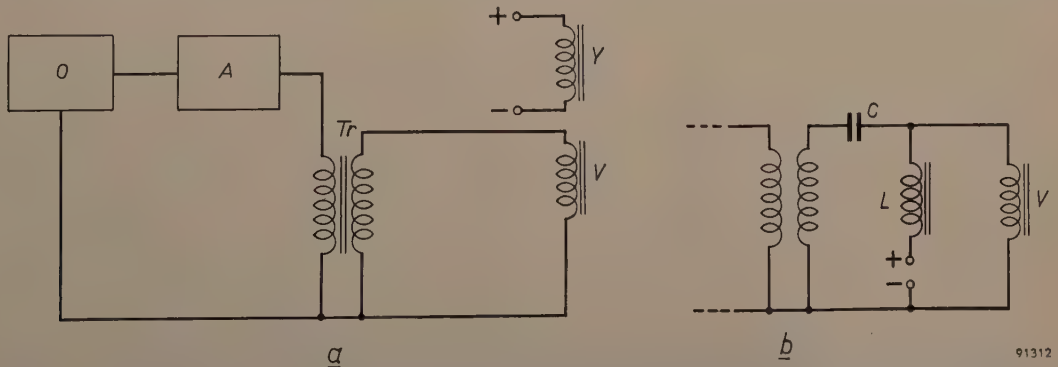

Fig. 8. *a*) Block schematic diagram of drill vibrator drive system for the lower-power drill. *O* variable frequency oscillator, *A* power amplifier, *Tr* step-down output transformer, + and − terminals for D.C. supply for polarizing field, *V* transducer, *Y* yoke. *b*) In the high-power drill a blocking capacitor *C* and an L.F. choke *L* are added, whereby drive and D.C. polarizing supply can be fed to a single winding on the transducer.

amplifier is matched, through a step-down transformer designed to handle the chosen frequency efficiently, to the transducer load, which can be varied as necessary merely by adjusting the number of turns on the energizing coil. Polarization for the transducer is provided by completing the magnetic circuit of the transducer with a yoke of high permeability laminations supported sufficiently close to, but not touching, the vibrating member and on which is wound a separate coil carrying direct current from a suitable low-voltage supply as shown in fig. 8*a*. The velocity transformers, exponentially tapered, which amplify the vibrations obtained at the transducer face, have been shown in fig. 5. The required drilling tip can be screwed or soldered to the end. The complete drill head is mounted in a precision drill stand with arrangements to enable the drill to rest on the work with the necessary light pressure.

The transducer employed in the larger (2 kW) machine is built from nickel laminations of the window type described above. Biasing and drive currents pass through the same winding (see fig. 8*b*). A square stack (*V*) of these laminations (*fig. 9*) is brazed to a tapered mounting stub (*B*) and is subsequently consolidated into a solid stack using a resin cement. The complete transducer is supported by a nodal flange at the lower end of the cooling jacket (*J*) and may be raised and lowered along low-friction ball slides (*S*) by the rack and pinion mechanism (*R*). The weight of the transducer provides too great a static load for many drilling operations, and may be counter-balanced by means of an adjustable lever and weight system (not shown in fig. 9).

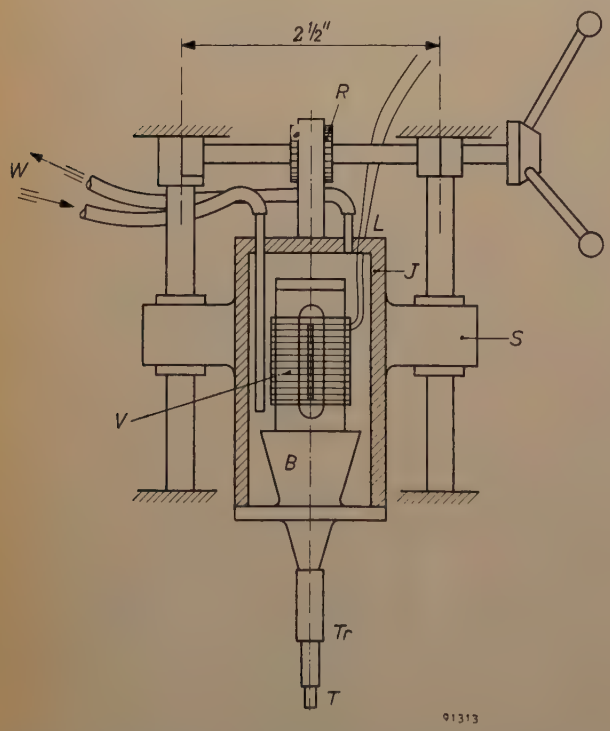

Fig. 9. Essentials of the high-power ultrasonic drill. *S* low-friction ball slides, *J* water jacket, *L* leads to transducer windings, *R* rack and pinion mechanism, *W* water connections, *V* transducer, *B* $\lambda/2$ mounting stub, *Tr* double $\lambda/4$ cylindrical velocity transformer, *T* tool.

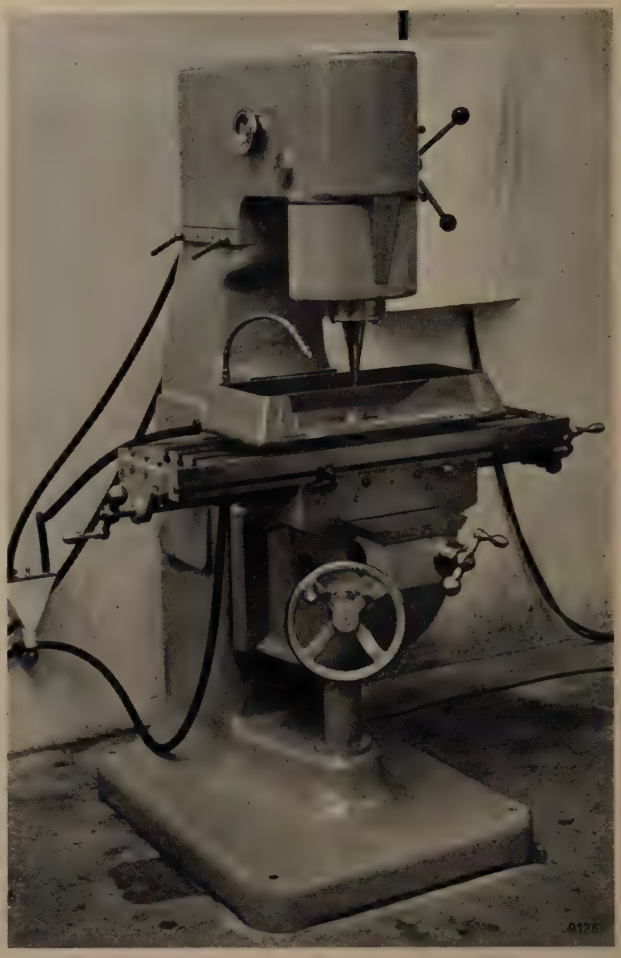

Fig. 10. Mullard high-power drill mounted on a standard type of machine-tool base, with moveable work table.

The complete drilling head is mounted above a work table closely resembling that of a standard milling machine. This enables the work to be moved accurately along the three rectangular coordinate axes, thus giving the machine some of the qualities of a jig borer.

Tools are carried at the lower end of a second velocity transformer (*Tr*) which screws on to the mounting stub. A photograph of the complete machine is shown in *fig. 10*. A close-up of a tapered velocity transformer and tool is shown in *fig. 11*.

Applications

The most valuable applications of the vibration machining technique arise from the fact that holes and patterns of intricate shapes can be cut in any brittle material.

Materials prepared by sintering techniques are often difficult to machine by conventional methods. Normally, sintered parts are pressed to shape before firing, so that the least possible amount of machining has to be undertaken on the sinter. Ultrasonic machine tools enable all manner of intricate shapes to be cut successfully in the fully-sintered state. Applications include the cutting of holes, slots and depressions in ceramics and sintered carbides.

Images and patterns may be simply and rapidly produced by the new method, the tool being merely the reverse impression of the required image, produced in a suitable metal. Since the chipping of the work is on such a small scale, extremely fine detail can be reproduced accurately. For working glass, ceramics and materials of comparable hardness, many impressions can be made from a single tool before tool wear results in any appreciable loss of definition in the image. The technique can of course be used to make dies for medallions or coins, in sintered carbides or die steels. In such materials, tool wear is always considerable so that it is necessary to use both roughing and finishing tools. *Fig. 12* shows photographs of cuts in tungsten carbide and glass by this technique.

Sapphire, ruby and agate are machined very rapidly; consequently the time required for the manufacture of jewel bearings for watches and precision instruments can be reduced considerably. In such applications, the major operation consists in cutting out small discs from thin sheet material. As the required dimensions are very small, it is possible and indeed for economic reasons necessary to use a multiple tool capable of blanking out a large number of discs in a single operation. The tool actually used in a typical job of this sort consisted of a cylindrical piece of mild steel rod $\frac{3}{8}''$ long, $\frac{5}{8}''$ diameter, having 35 holes each 1.6 mm diameter drilled into it longitudinally. To ensure a parallel-sided cut, and to avoid chipping at the edges as the tool penetrates the work, the sapphire sheets are fixed rigidly to a glass backing plate and the tool is allowed to penetrate not only the work but also some distance into the backing material. In this way discs have been cut to a dimensional accuracy of ± 0.001 inch on diameter in about one minute from sapphire sheets 1 mm thick.

An important application is in the manufacture of transistors, since the materials used, germanium and silicon, are brittle enough to be easily machined by this method. For slicing bulk crystals, the most economical technique is to use a multiple slicing

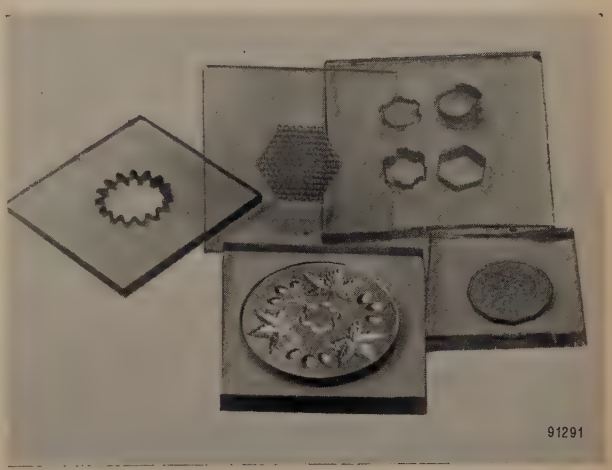

Fig. 12. Holes and bas-relief patterns of various shapes cut in sintered tungsten carbide (above) and glass (below).

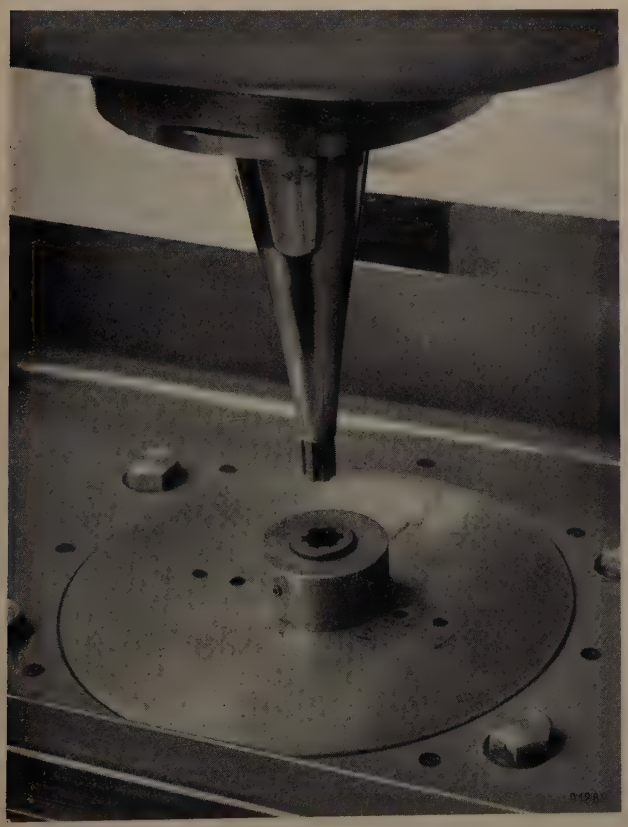

Fig. 11. Close-up photograph of a velocity transformer and tool fitted to the high-power drill.

tool in the form of a set of parallel blades fixed rigidly in a supporting frame with the required separation. For cutting out the small discs required in transistor manufacture, a multiple blanking technique is used, similar to that described above. This is a valuable production technique, a considerable advance on the use of rotary diamond-impregnated tools.

Considerable difficulties exist in applying conventional techniques to drilling very small holes and depressions in brittle materials. This applies even to round holes. Experiments have shown that extremely small holes, down to at least 0.007 inch diameter, can be cut on the vibration machine provided suitable precautions are taken. To apply the very light static loading required, the drill is preferably made immovable and the load applied by supporting the workpiece on a guided platform, itself supported on a light spring. The load can in this way be set by adjusting the compression of the spring. In cutting small round holes where the circularity is important it is an advantage to rotate the workpiece during the drilling. There is no advantage in rapid rotation and a rate of a few revolutions per second is adequate. The rotation also helps considerably in circulating the abrasive under the tool. As examples of the drilling of small holes to close tolerances we may mention the manufacture of diamond wire-drawing dies and, again, in transistor manufacture.

A useful technique for drilling in places which would normally be inaccessible is to couple the vibrations from the transformer to the tool through a flexible coupling, in the form of a thin wire of a material of suitable high fatigue strength and low loss characteristics. This technique also allows the work to be carried out at considerable distances from the transducer when suitable wire is used. Experience shows that this technique is a very convenient one for drilling small holes rapidly when the operation must be done manually and when positional accuracy is not important. The vibrations are transmitted, with very little attenuation, largely as axial vibrations with only a small shear component, even when the wire is bent so sharply that the radius of curvature is small compared with the wavelength. This suggests an interesting application of this technique: the drilling of *curved* holes — holes with axes bent in any desired way and of any required section. Many actual cuts of this sort have been made in glass.

A field of some promise for ultrasonic techniques is in dental drilling. Investigations have been made in this direction using the above-mentioned wire transmission lines in conjunction with remote transducers and also using miniaturized transducers.

The vibration machining technique is likely to have its greatest application in the field of die making, since the materials used — hardened steels, sintered carbides and diamonds — are brittle enough to be machined quite rapidly by these methods. Die making by conventional methods is generally a very protracted process involving lengthy periods of lapping, much of which must be done manually using expensive diamond powder and diamond-impregnated tools. Moreover, dies of any complexity must generally be made up in a number of segmental sections and are therefore inherently weak. By using the ultrasonic technique these difficulties are overcome. The most complex shapes can be cut out comparatively rapidly in one piece, using inexpensive boron-carbide abrasive, except where diamonds themselves are to be cut. During the investigations recorded in this article, a great number of holes of all shapes have been cut in tungsten carbide. Extrusion dies and wire-drawing dies require a tapering lead-in and exit portion which can readily be produced on the ultrasonic machine using an appropriate tool of tapering section. However, in large carbide dies where stock removal is considerable, machining time can be saved by sintering the carbide blank roughly in the required form (but undersized on all internal dimensions) and using the vibration technique merely for sizing. If this is done it may be possible to reach the required dimensional tolerances in only one operation.

The second part of this article will deal in some detail with cutting speeds, accuracy and surface finish.

Summary. This article gives an introduction to the technique of drilling by means of ultrasonic vibrations. The actual cutting action consists of a continuous chipping of the work by abrasive particles in suspension, fed between tool and work. A vibration frequency in the ultrasonic region ($\sim$ 20 kc/s) is used, both for silent operation and in order to get reasonable cutting rates. Piezomagnetic (magnetostrictive) transducers are particularly well suited for generating the vibrations. Two types of laminated metal transducers are described — a bar-type and window-type. These are used in two ultrasonic drills developed by the Mullard Research Laboratories, the former in a small 50 W drill and the latter in a larger water-cooled 2 kW model. The associated velocity transformers are described in some detail: these are resonant stubs, fixed to the transducer and holding the tool, which serve to amplify the vibrations at the tool face. Ultrasonic drilling can be applied only to hard, relatively brittle materials. Among the applications are cutting, the drilling of holes of any cross-section and the production of bas-reliefs, in such materials as glass, tool steel, sintered carbides, ceramics and precious stones. Using a mechanical transmission line of flexible wire it is possible to drill holes in otherwise inaccessible places; even curved holes can be bored. Some of the other applications mentioned are the manufacture of blanking dies and wire-drawing dies and of precious-stone bearings for watches and instruments. The use of ultrasonic machining in transistor manufactore and for dental drilling are also mentioned. A second article will discuss in more detail cutting speeds, accuracy and surface finish.

HERBICIDE MANUFACTURE IN THE PHILIPS-ROXANE FACTORY AT AMSTERDAM

The firm of Philips-Roxane markets a number of insecticides and other chemicals for agriculture and horticulture. One of these is the herbicide 2,4,5 trichloroacetic acid (see inset formula) referred to as 2,4,5-T, used to combat weeds [1]). The above photograph shows the plant in which this chemical is synthesized. Hexachlorohexane is changed into a dichlorophenol in the autoclave just visible at bottom left of the photograph. The 2,4,5-T is produced in two further stages: the reaction of the dichlorophenol with monochloroacetic acid and the replacement of a certain H atom in the benzene ring by a chlorine atom. By reaction with suitable alcohols (apparatus to left of steps) the 2,4,5-T is then made into an ester, which is the form in which it is used.

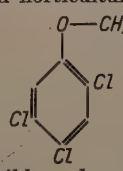

[1]) See Philips tech. Rev. **16**, 356, 1954/55; **17**, 295, 1955/56.

SWITCHING TIME OF FERRITES WITH RECTANGULAR HYSTERESIS LOOP

by H. van der HEIDE, H. G. BRUIJNING and H. P. J. WIJN.

621.317.4:538.23:621.318.134

The use of ferrites with rectangular hysteresis loop as magnetic "memory" elements in electronic computers calls for a means of determining as a function of time the reversal of magnetization caused by current pulses. A method of measuring this process is described in the present article. Some results are given and their possible interpretation is discussed.

This article on ferrite cores with a rectangular hysteresis loop, as employed in electronic computers, may be regarded as a sequel to a previous article on this subject [1]). That article dealt mainly with the static properties of ferrite cores, whereas we shall now be concerned with their dynamic behaviour. The ferrite cores (*fig. 1a*) are activated by rapid current pulses which have a more or less square wave-form, i.e. they rise very rapidly (commonly in about 0.2 microsecond) to a certain value, remain constant at that value for some time and then fall rapidly to zero again. When a current pulse of this kind, shown diagrammatically in fig. 1*b*, excites a magnetic field in a ferrite, it is found that in most cases the change in magnetization produced by this field cannot follow the increase in the current: this change only begins to become clearly noticeable after the current (the field) has been at its maximum value for some time.

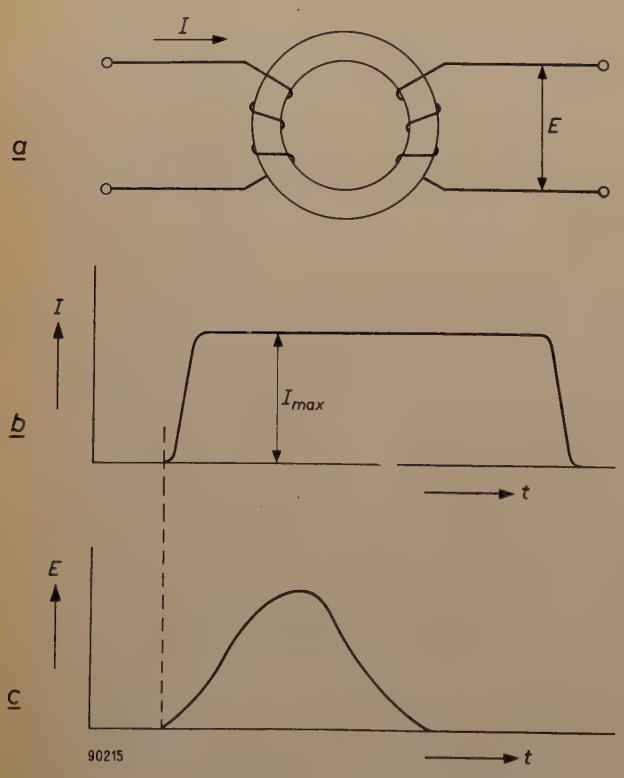

Fig. 1. Ferrite core (*a*) with two windings. A current pulse (*b*) in the first winding gives rise to a voltage pulse (*c*) in the second winding.

The change of magnetization in the core consists usually in the reversal of the magnetization, for example from negative remanence to the positive magnetization corresponding to the magnetic field applied. (In the following we shall refer to this simply as *reversal*.) The ultimate state of magnetization that is set up, that is, after the passage of the current pulse, is, in the cases in which we are interested, always symmetrical with respect to zero, e.g. from negative remanence to positive remanence.

It is obvious that the duration of the pulse must be longer than the time needed for this reversal, which we shall call the reversal time. If we increase the amplitude of the pulse, the reversal will be more rapid and the reversal time shorter. If we reduce the amplitude the reversal time will be longer. The reversal time does not, however, become continuously longer with decreasing field, for if the magnetic field is too weak, e.g. smaller than the coercive force of the ferrite, the reversal will be only from one non-saturation value to the opposite value and will finally be quite impossible. It is precisely upon this that the practical use of ferrite cores is based (see I). The time for the "non-saturation reversal", which takes place at low field strengths, again appears to be shorter than the longest time needed for almost complete reversal, so that if the reversal time is plotted against the current or the field, a maximum is found in the reversal time. Only that part of the curve at the right of the maximum is of practical importance, for the left part of the curve refers to pulses which do not lead to a full reversal. The maximum reversal time is found approximately at that field strength at which the "rectangularity" or "squareness ratio" (see I) is greatest. For ferrite

[1]) H. P. J. Wijn, E. W. Gorter, C. J. Esveldt and P. Geldermans, Conditions for square hysteresis loops in ferrites, Philips tech. Rev. **16**, 49-58, 1954/55; referred to in this article as I.

rings used as memory elements in computers, therefore, a field strength is applied that corresponds roughly to this maximum reversal time.

In the following we shall reserve the term "switching time" for the maximum reversal time.

Measurement of the reversal time

The method of measuring the reversal process is in principle as follows. A ferrite ring is given two windings as shown in fig. 1*a*; a current pulse is passed through the primary winding (fig. 1*b*) which magnetizes the ring or causes a reversal of the magnetization. As a result of this, a variable voltage is induced in the secondary winding (fig. 1*c*), the instantaneous value of which is proportional to dB/dt (B is the magnetic induction). The area under the curve is thus a measure of the change of induction. The voltage can be viewed directly on an oscilloscope. The measurement naturally requires this process to be repeated at certain regular intervals, and the current pulses employed must be alternately positive and negative. Two primary windings can also be used, wound in such a way that pulses fed to them alternately magnetize the ring first in one direction and then in the other.

The current pulses are commonly generated by valve circuits. Only small ferrite rings can then be activated with adequate rapidity, because the power available is usually rather low. The amount of work needed for a single reversal is proportional to

$$V H \Delta B,$$

where ΔB is the change of induction, H the magnetic field strength and V the total volume of the ferrite core.

In the investigation described here, measurements were carried out not on the small rings used in memory circuits but on fairly large rings (e.g. 28 mm outside diameter, 20 mm inside diameter and 4 mm thick). Some of these, moreover, had a fairly high coercive force (e.g. $\mu_0 H_c = 10 \times 10^{-4}$ Wb/m² [$H_c = 10$ Oe]). Since ΔB lies almost invariably between 0.2 and 0.8 Wb/m² [2000-8000 gauss], the product $VH\Delta B$ is too large to permit the successful use of normal amplifier valves. For this reason we employed RC discharges via hydrogen thyratrons (type PL 522) for generating the current pulses. In this way we were able to generate pulses of a power more than sufficient for our purposes. These pulses differ from those generated with the aid of vacuum tubes in that although they rise very steeply in the beginning, they have no sharply defined end. As we shall see later, this constituted no objection.

The basic diagram of the circuit used is shown in *fig. 2a*. Capacitor $2C$ is charged up to a voltage E via resistor R_t. When the thyratron T strikes, the discharge current I flows via the thyratron, through the winding of the ferrite ring and the RC circuit.

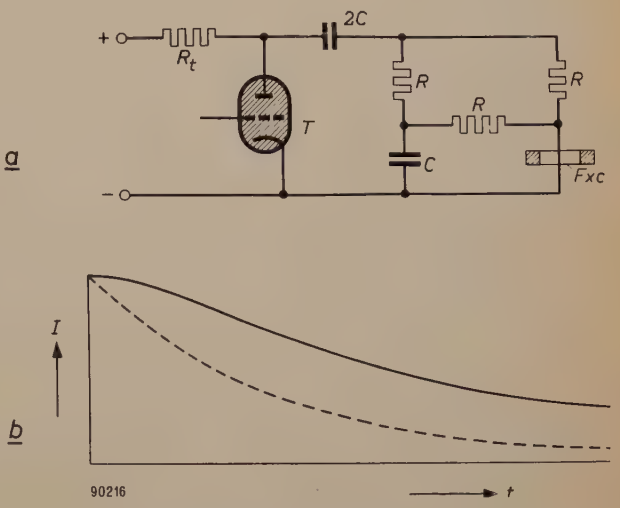

Fig. 2. *a*) Simplified diagram of the circuit used. When thyratron T strikes, capacitor $2C$ discharges and sends a current pulse through the winding on the ferrite core *Fxc*.
b) Dashed: current curve of an ordinary RC discharge according to $I = (E/R) \exp(-t/2RC)$. Fully drawn: current pulse supplied by the circuit in (*a*), according to $I = (E/R)\{(a+2)\exp(at/RC) + (b+2)\exp(bt/RC)\}$, in which $a = \frac{1}{2}(-3+\sqrt{3})$ and $b = \frac{1}{2}(-3-\sqrt{3})$.

The form of the current pulse through the coil is as shown in fig. 2*b*. If the circuit had only consisted of capacitor $2C$ and resistor R on the extreme right, a curve according to

$$I = \frac{E}{R} e^{-t/2RC}$$

would have been obtained, as shown by the dashed line in fig. 2*b*. Since, however, in the actual circuit capacitor C is first charged up and subsequently discharged via the ferrite core winding, a flatter current curve is obtained; in fact, with the RC network shown here, the resultant curve is exactly horizontal at the beginning, as shown in the fully-drawn line of fig. 2*b*. In this case, the current I falls less than 4% in the time $\tau = \frac{1}{4}RC$. For the frequently used values $C = 6000$ pF and $R = 6500\ \Omega$, this time comes to approximately 10 μs. For almost all the ferrites measured, the reversal times are much shorter than 10 μs; in fact, they are usually shorter than 3 μs.

As we have seen, field pulses are needed in both directions, and these are obtained by duplicating the arrangement given in fig. 2*a*. *Fig. 3* shows the complete circuit, which functions as follows.

During the half cycle in which the anodes of the diodes are positive, the two capacitors $2C$ are charged up by the 50 c/s transformer. A special pulse generator then supplies the grid of one of the thyratrons T with a voltage pulse which causes the

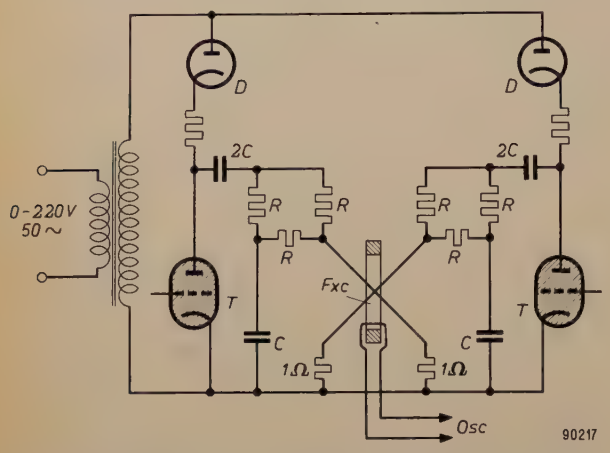

Fig. 3. More detailed circuit diagram. D diodes, other symbols as in fig. 2. The current pulses are synchronized with the mains frequency, so that no D.C. supply is required. The two halves of the circuit operate alternately and produce successive fields of opposite sign in the ferrite core Fxc.

thyratron to strike, as a result of which a current pulse as shown in fig. 2*b* flows through one winding of the ferrite ring. One cycle later the same process is repeated with the other thyratron, the result of which is a current pulse in the second winding, which excites an opposing field in the ferrite ring. For the purpose of measuring the voltage pulse there is a third winding, connected directly to an oscilloscope.

The repetition frequency of each pulse train is thus 25 c/s. Now the duration of the voltage pulses may be as short as 2 μs, whilst they are displayed on the oscilloscope at intervals of 40 000 μs. It would therefore be quite useless to apply the pulse to an oscilloscope with the normal linear time base, generated by a sawtooth voltage. For this reason use is made of a "pulse oscilloscope" (type GM 5660) the time base of which is triggered only during a time interval that is short compared with one cycle of the repetition frequency. The effect of this is the same as if the time base were to extend far beyond the screen. The horizontal movement of the light spot is synchronized with the pulses by means of an extra signal from the external pulse generator mentioned above. From the fact that the electron beam describes a pattern on the screen during only a very small fraction (on an average 10^{-4}) of the total time, it follows that the pattern cannot be very bright. In an undarkened room the observer must therefore view the patterns under a black hood, in the manner of a photographer.

Having now obtained the oscillogram of the voltage pulse of the ferrite at a given pulse current, we can proceed to measure, for example, the total duration and the maximum amplitude of the pulse. If is often useful, however, to determine the complete variation of the voltage as a function of time. This might be done by photographing the oscillogram, but it is easier to read off a few points of the curve on an illuminated scale, previously calibrated in time and voltage. For adjusting the time scale, a voltage source in the oscilloscope itself was used, which supplies an alternating voltage at a frequency of 1 Mc/s; for the voltage scale a special and very simple square-wave generator was used.

In order to measure the pulse current as well, resistors of 1 Ω were connected in series with the two primary windings of the ring. The voltages across these resistors were also measured on the oscilloscope. In the RC circuit, C had the value 6000 pF (i.e. $2C = 12\,000$ pF) and three values were used for R, viz. 12 000 Ω, 6500 Ω or 960 Ω. These resistors are formed of arrays of carbon resistors, consisting of 8 annular groups of 10 parallel resistors in series. Each array R is thus cylindrical in form, about 7 cm in diameter and about 30 cm in length. This measure is necessary in the first place to keep self-inductances as low as possible, and also to distribute the dissipated power (70 W at 15 kV) over a large number of carbon resistors. As can be seen from fig. 3, six such arrays are needed for the six resistances R.

Results of measurements

Fig. 4 shows three secondary voltage pulses as measured on ferroxcube 6A, for fieldstrengths $\mu_0 H = 1.3$, 1.85 and 2.6×10^{-4} Wb/m² [$H = 1.3$, 1.85 and 2.6 Oe]. What is immediately noticeable

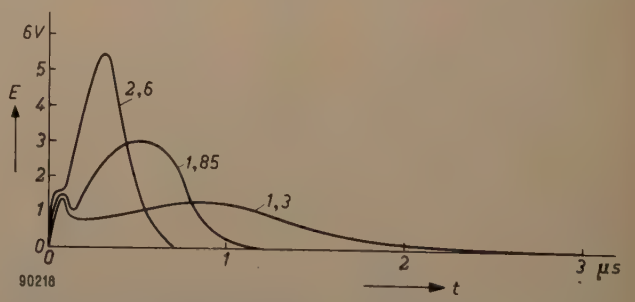

Fig. 4. Voltage pulses measured on ferroxcube 6A. In order of increasing magnitude: $\mu_0 H = 1.3$, 1.85 and 2.6×10^{-4} Wb/m².

is that the voltage pulse can show two separate maxima; this points to two different processes in the reversal. For these ferrites with rectangular hysteresis loop the first maximum always represents

a small percentage of the total area under the curve and hence of the change in magnetization ΔB. We see that at greater field strength the voltage pulse has a greater amplitude and a shorter duration. The duration τ of a voltage pulse is defined [2]) as the time (counted from the beginning of the current pulse) which elapses before the voltage has dropped to 10% of the maximum value; for the maximum value the second peak is considered.

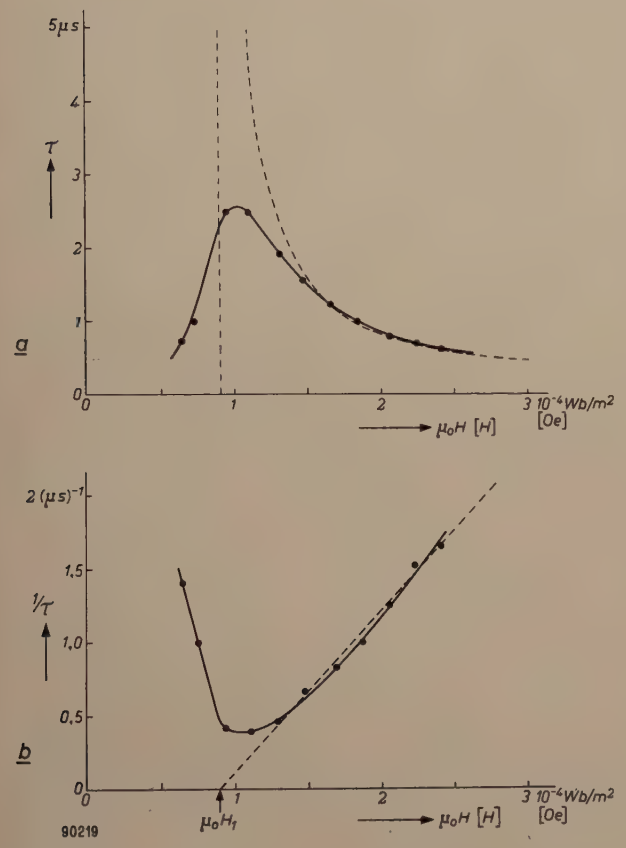

Fig. 5. *a*) Reversal time τ as a function of the pulse field strength H, for ferroxcube 6A.
b) Reciprocal of reversal time, $1/\tau$, as a function of H, for ferroxcube 6A. The slope of the straight line is determined by $s = \mu_0(H-H_1)\tau$.

Fig. 5a shows the reversal time as a function of the corresponding field strength H. We can see the maximum in τ mentioned in the introduction. After $\mu_0 H \approx 1 \times 10^{-4}$ Wb/m² [$H \approx 1$ Oe] the curve becomes approximately a rectangular hyperbola (dashed):

$$\mu_0(H-H_1)\tau = \text{const.} = s.$$

If we plot the reciprocal of τ as a function of $\mu_0 H$, as in fig. 5*b*, the result is a straight line [3])[4]), the slope of which is given by the constant s. The significance of H_1 (often referred to in the literature as H_0) is immediately apparent from the figure. In the case of ferroxcube 6A, considered above, the resultant values are $\mu_0 H_1 = 0.9 \times 10^{-4}$ Wb/m² [$H_1 = 0.9$ Oe] and $s = 0.9 \times 10^{-4}$ μs Wb/m² [0.9 μs Oe].

In cases where dB/dt after the first sharp peak falls off and shows no further maximum (see fig. 8), it is difficult to decide on clearly defined values of τ. It is therefore useful to introduce another definition of the reversal time, in order to be able to define clearly the reversal time for arbitrary forms of voltage pulse, e.g. of ferrites which have no rectangular loop at all. For this purpose we can take twice the time in which the reversal process as regards the change in induction (ΔB) is half completed. The reversal time τ' so defined can best be established by determining at what point a time-integrated pulse curve has reached half of its final value (*fig. 6a*). The integral curve can be determined graphically from a plotted pulse curve, but it is simpler and quicker to observe the electrically integrated curve on an oscilloscope. Fig. 6*a* shows integral curves found in this way for ferroxcube 6A at a number of pulse field strengths. Fig. 6*b* gives the reciprocal of the determined values of τ' as a function of the pulse field strength H. It can be seen that, like $1/\tau$, $1/\tau'$ also shows a minimum. In fig. 6*c* the total change in induction, which can very easily be found by this method, is plotted against the pulse field strength H.

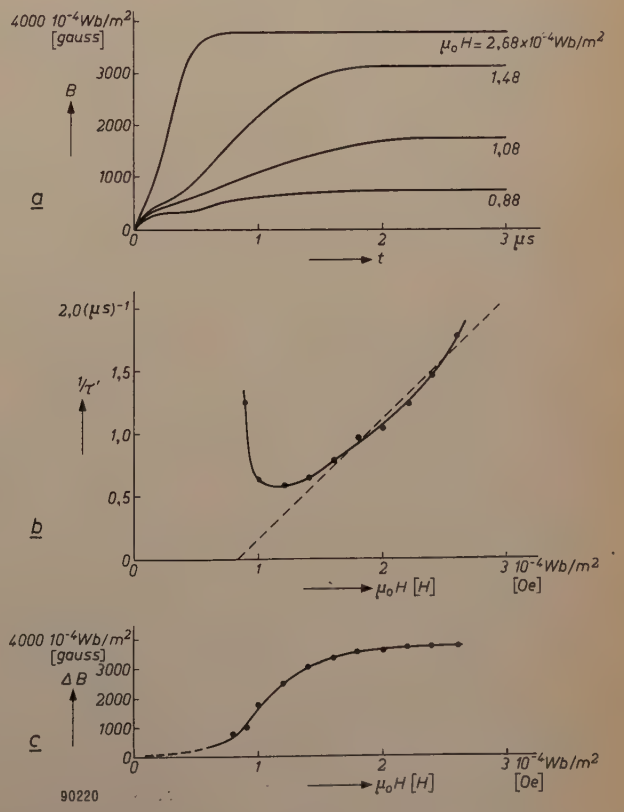

Fig. 6. *a*) Integral curves $B = f(t)$ for ferroxcube 6A, for various values of $\mu_0 H$.
b) Reciprocal of τ', derived from (*a*), as a function of $\mu_0 H$.
c) Total change of induction ΔB as a function of $\mu_0 H$.

[2]) N. Menyuk and J. B. Goodenough, J. appl. Phys. **26**, 8-18, 1955.
[3]) J. K. Galt, Bell Syst. tech. J. **33**, 1023-1054, 1954.
[4]) J. Wylen, Trans. A.I.E.E. **72**, Part I, 648-656, 1953.

Effects of the chemical composition

In article I some experimental compositions of ferrites with rectangular hysteresis loop were mentioned, together with their various properties. The pulse measurements described in the present article were carried out on these and other ferrites. It is found that the great majority of ferrites with the rectangularity and the coercive force usual for switching elements all have a "reversal constant" $s = \mu_0(H-H_1)\tau$ of the same order of magnitude. A synopsis of these values is given in *Table I*.

The most striking deviations from the normal values of s and τ_{max} are shown by $Co_{0.1}Fe^{II}_{0.9}Fe^{III}_2O_4$ and $MnFe_2O_4$. The pulse characteristics of these compounds are given in *figs 7* and *8*. As a general rule it appears that the switching time is longer the better the rectangularity of the hysteresis loop, i.e. the larger the squareness ratio $R_{s\,max}$ (see I). Having regard to this rule, $C_{0.1}Fe^{II}_{0.9}Fe^{III}_2O_4$ also fits well into the normal pattern. As a result of the heat treatment in a magnetic field, the squareness ratio in this case is particularly large;

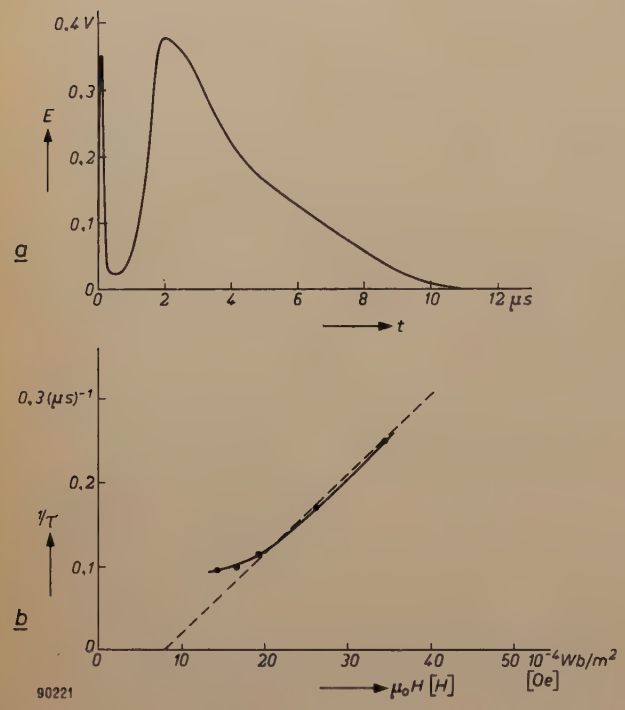

Fig. 7. *a*) Voltage pulse measured on a core of $Co_{0.1}Fe^{II}_{0.9}Fe^{III}_2O_4$ at $\mu_0H = 19.5\times10^{-4}$ Wb/m². *b*) $1/\tau$ as a function of μ_0H; in this case s is particularly large.

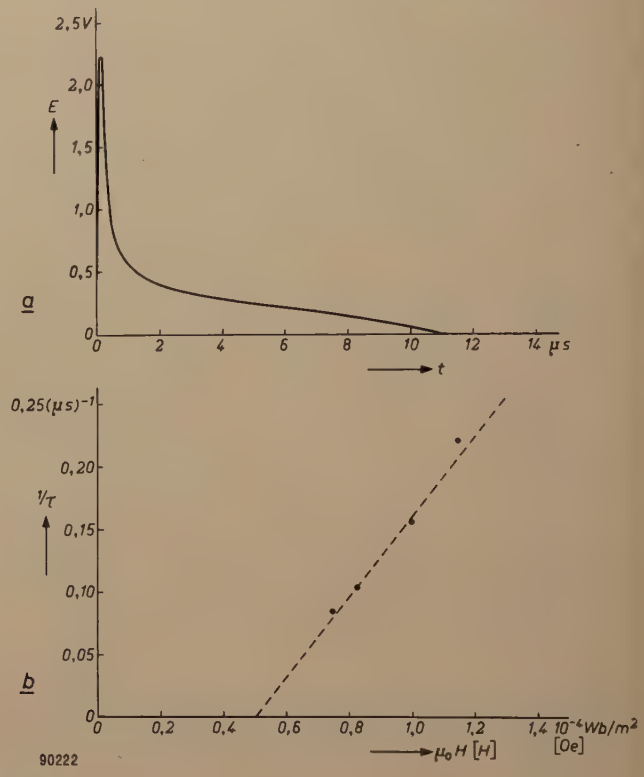

Fig. 8. *a*) Voltage pulse measured at $\mu_0H = 0.83\times10^{-4}$ Wb/m² on a core of $MnFe_2O_4$. There is no second peak. *b*) $1/\tau$ as a function of μ_0H.

Table I. Switching times and other properties of various ferrites with a rectangular hysteresis loop: τ_{max} longest possible reversal time (switching time); for μ_0H_1 see fig. 5*b*; s slope of $1/\tau = f(\mu_0H)$; $R_{s\,max}$ maximum squareness ratio corresponding to induction B_m obtained at μ_0H_{max}; B_r induction in remanent state.

Ferrite	τ_{max} μs	μ_0H_1 10^{-4} Wb/m² [H_1 in oersted]	s μs×10^{-4} Wb/m² [μs× oersted]	$R_{s\,max}$	B_r/B_m	μ_0H_{max} 10^{-4} Wb/m² [H_{max} in oersted]
Ferroxcube 6A	2.5	0.9	0.9	0.8	0.92	1.5
$Cu_{0.25}Mn_{0.75}Fe_2O_4$	2.2	0.85	0.8			
$(MgO)_{0.5}(MnO_{1+\delta})_{0.875}Fe_2O_3$	1.3	1.4	0.9	0.75	0.88	1.5
$Mg_{0.6}Ni_{0.4}Fe_2O_4$	2.5	3.6	2.2	0.8	0.90	2.2
$Li_{0.47}Ni_{0.06}Fe_{2.47}O_4$	0.6	~ 2.2	~ 1	0.85	0.93	
$Co_{0.1}Fe^{II}_{0.9}Fe^{III}_2O_4$	10	8	105	0.95	0.97	10
Ferroxcube 4A	0.4			~ 0	~ 0.5	0.3
$MnFe_2O_4$	11	0.5	3.2	0.8	0.9	0.5

the same applies to the switching time. The only exception is $MnFe_2O_4$. In this case the form of the voltage pulse (fig. 8*a*) differs considerably from that mostly found. No explanation is yet known for this deviation; it may perhaps have some connection with a systematic inhomogeneity in the ferrite.

Effect of mechanical stress

In article I the case was discussed of a glass ring shrunk on to a ring of ferroxcube 4A. As a result of the stress thus exerted on the ferrite, a great improvement was obtained in the rectangularity of the hysteresis loop (see also [5])). The same object was achieved in the present investigation by enclosing a ferrite ring in a rubber ring, and by entirely enclosing the latter in the manner shown in

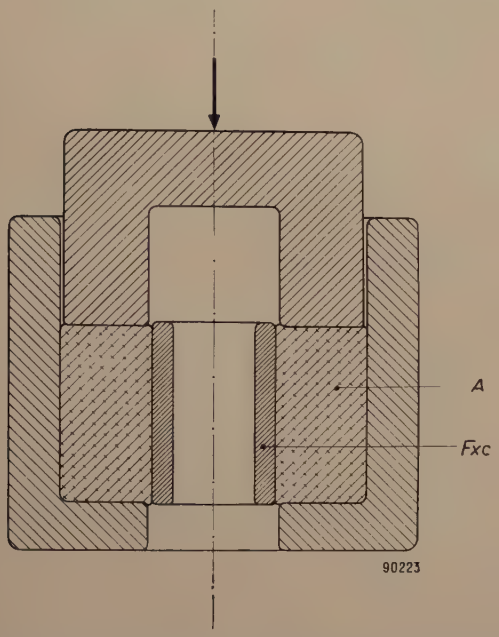

Fig. 9. Schematic diagram of a device for applying a tangential stress to a ferrite core *Fxc* by compressing a rubber ring *A*.

fig. 9 and applying pressure to it. With this method the magnitude of the pressure can only be determined comparatively. In *Table II* are listed the

Table II. Switching times and other properties of ferroxcube 4A for various values of mechanical stress applied parallel to the direction of the magnetic field.

Stress	τ_{max} μs	$\mu_0 H_1$ 10^{-4} Wb/m² [H_1 in oersted]	s μs × 10^{-4} Wb/m² [μs × oersted]	$R_{s\,max}$	B_r/B_m
None	0.4	—	—	0	0.5
Moderate	1.8	0.6	0.7	0.4	0.7
High	6	1.2	1.8	0.7	0.9
Very high	8	1.6	2.2	0.75	0.95

[5]) H. J. Williams, R. C. Sherwood, M. Goertz and F. J. Schnettler, Trans. A.I.E.E. **72**, Part I, 531-537, 1953.

quantities τ_{max}, s, $R_{s\,max}$ and B_r/B_m; *fig. 10* shows the form of the voltage pulses for a zero pressure and for three increasing values of the pressure. As can be seen, the effect on the squareness ratio

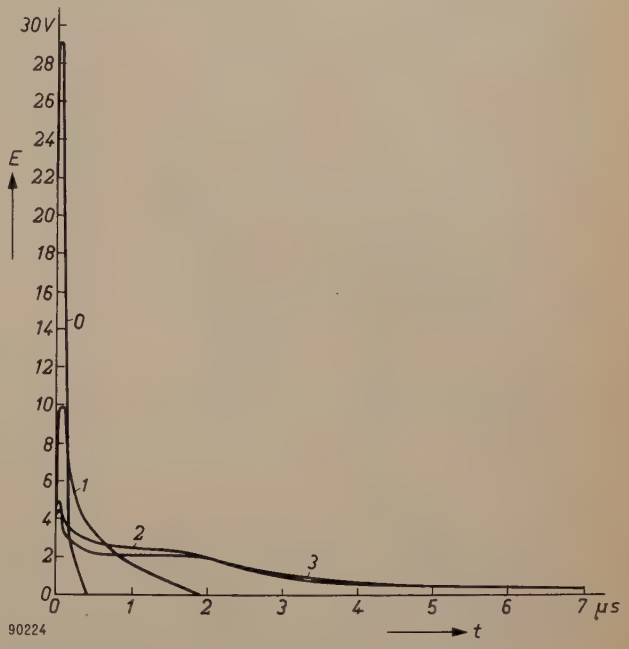

Fig. 10. Voltage pulses measured in ferroxcube 4A at various values of mechanical stress, increasing in the order of curves *0* to *3* and corresponding to the four values given in table II.

$R_{s\,max}$ and on the pulse duration τ_{max} is surprisingly pronounced. As a result of the pressure, τ_{max} is increased by a factor of 20. All this is in good agreement with the above rule that the switching time becomes longer as the hysteresis loop becomes more rectangular.

Effect of the temperature

It remains to inquire into the temperature-dependence of these switching phenomena. The various properties of ferrites are very differently affected by changes in temperature: for example, the magnetization saturation [6]) does not usually change very much in a small temperature range, the initial permeability can change much more, while the electrical conductivity usually undergoes a very pronounced change.

In *fig. 11* the reciprocal of τ is plotted as a function of $\mu_0 H$ for $Cu_{0.25}Mn_{0.75}Fe_2O_4$, for various temperatures. In *fig. 12* the values found for s and $\mu_0 H_1$ are plotted against temperature. In the temperature range from —100 to +250 °C the field-strength H_1 changes roughly in the same manner as the coercive force. The reversal constant s does

[6]) J. J. Went and E. W. Gorter, The magnetic and electrical properties of ferroxcube materials, Philips tech. Rev. **13**, 181-193, 1951/52.

not change much either; it decreases by a factor of 2. This behaviour of the reversal constant is a clear indication that the inertia of the reversal is not due to eddy currents, as it is in metallic ferromagnetic materials. One might at first think that for

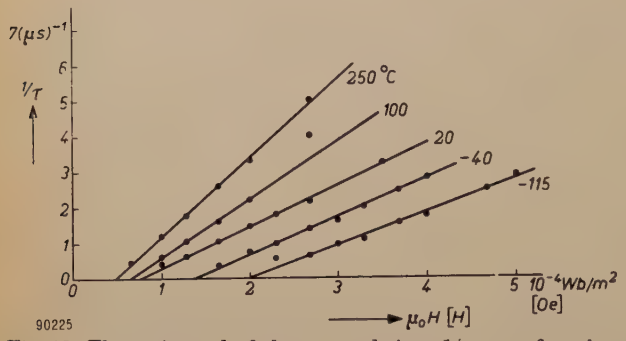

Fig. 11. The reciprocal of the reversal time, $1/\tau$, as a function of $\mu_0 H$, measured on a ring of $Cu_{0.25}Mn_{0.75}Fe_2O_4$ at various temperatures.

this ferrite, eddy currents could be the explanation, in view of the fact that the resistivity ϱ is only 1500 Ωcm, which is much lower than in most other ferrites. However, since the resistivity decreases exponentially with increasing temperature, we should expect, if the inertia of reversal were attributable to eddy currents, that s would rise sharply with temperature, instead of falling slightly. It may be mentioned in this connection that if the effect of eddy currents in metallic ferromagnetic materials is eliminated by using very thin laminations, it is also found that s varies only very slightly with temperature [7]).

We shall now inquire into the possible physical explanations of the time effects occuring in connection with reversal.

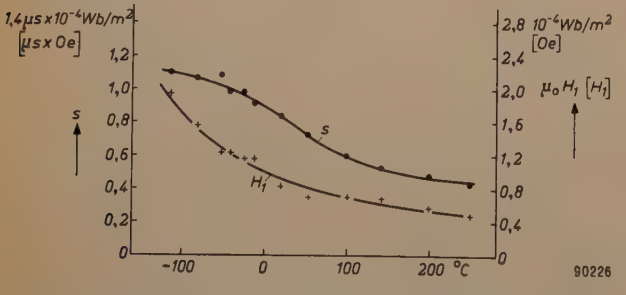

Fig. 12. Reversal constant s and $\mu_0 H_1$ as functions of temperature, measured on a ring of $Cu_{0.25}Mn_{0.75}Fe_2O_4$.

Interpretation of the observed phenomena

In attempting to explain these phenomena, we shall first consider the shape of the voltage pulse during the reversal. It is usually found that the secondary voltage shows a sharp peak, followed by a flatter maximum (figs 4 and 7). This second maximum is sometimes absent, in which case the voltage after the first peak merely falls off gradually and relatively slowly (fig. 8). For a closer analysis we shall start from the normal hysteresis loop in a slowly changing field. We shall divide the field H, as shown in *fig. 13*, into a static component (H_{st}) and a dynamic component (H_{dyn}), and we shall further assume that dB/dt, and hence the voltage E of the induced voltage pulse, is at each instant proportional to the instantaneous value of H_{dyn}.

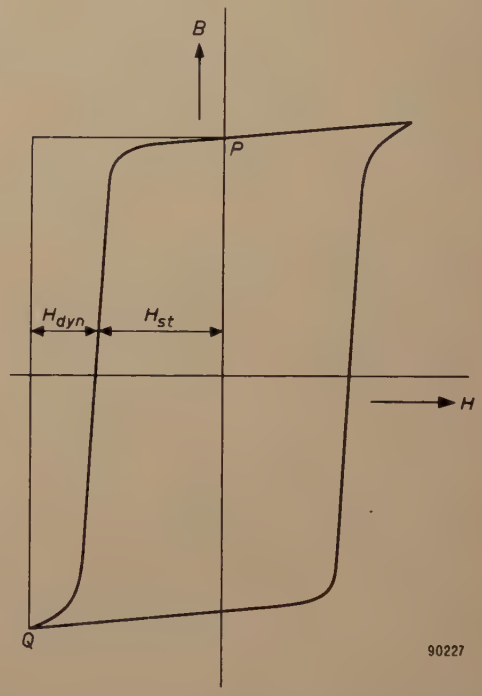

Fig. 13. Hysteresis loop indicating the definition of the dynamic field strength H_{dyn}; the sum $H_{dyn} + H_{st}$ is equal to the applied pulse field strength H.

The reversal takes place from point P to point Q. We can now replot a part of fig. 13 so as to obtain a curve of H_{dyn} as a function of B which, according to our assumption, also constitutes a curve of dB/dt as a function of B (on a different scale; *fig. 14a*). We take the reciprocal of dB/dt and thus obtain a new function (fig. 14*b*), viz. dt/dB as a function of B, which integrated to B (fig. 14*c*) gives t as a function of B. If the last curve is replotted in the more usual way, with t as abscissa (*fig. 15a*), we obtain B as a function of t. From this curve we can simply derive dB/dt as a function of t (fig. 15*b*). If our assumption that dB/dt is proportional to H_{dyn} is correct, the curve thus derived should correspond to the voltage pulse as obtained by measurement.

[7]) N. Menyuk, J. appl. Phys. **26**, 692-697, 1955.

In fact, the agreement of the theoretical pulse form with the measured form is, in most cases, by no means unsatisfactory. The first sharp peak is immediately apparent. (This is also explained by other workers in roughly the same way; see e.g. [8]).) The absence of the rise from zero is due to the fact that, in plotting the curves in figs 14 and 15, we took the ideal case of a rectangular current pulse (zero starting time). Moreover, the theoretical curve

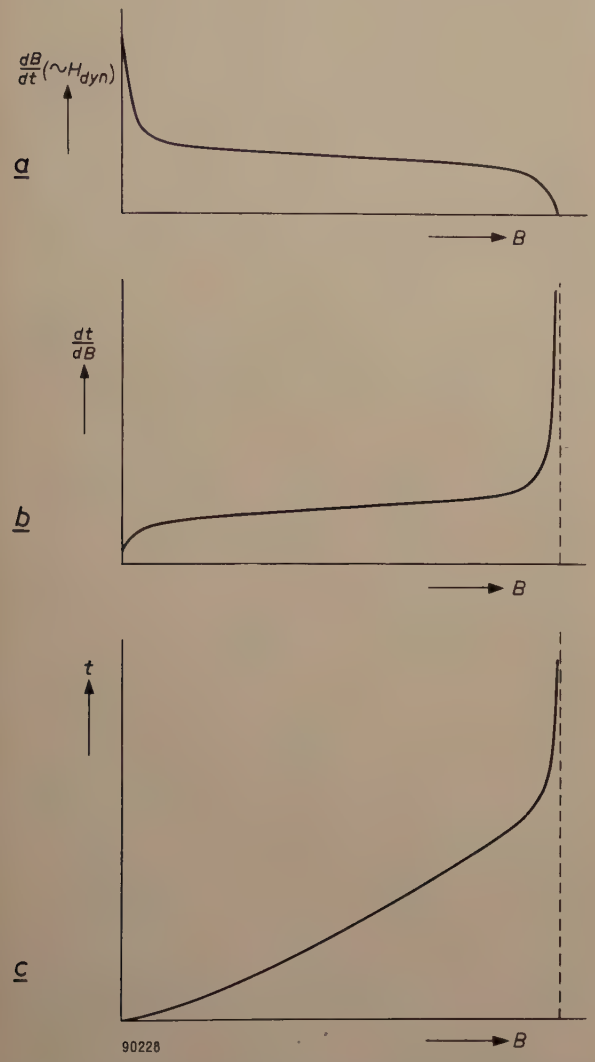

Fig. 14. *a*, *b* and *c*) Graphic derivation of t as a function of B from H_{dyn} as a function of B, assuming that dB/dt is directly proportional to H_{dyn}.

agrees well with the rule that the better rectangularity of the loop, the longer the reversal time (larger region where H_{dyn}, hence dB/dt, can be small, fig. 13). However, in no case is there a further rise of dB/dt after the first peak, whereas in practice this is very frequently observed. We might try to explain this qualitatively by the plausible assumption that the reversal caused by a rapid current pulse takes place according to a mechanism diffe-

[8]) M. Karnaugh, Proc. Inst. Rad. Engrs. **43**, 570-584, 1955.

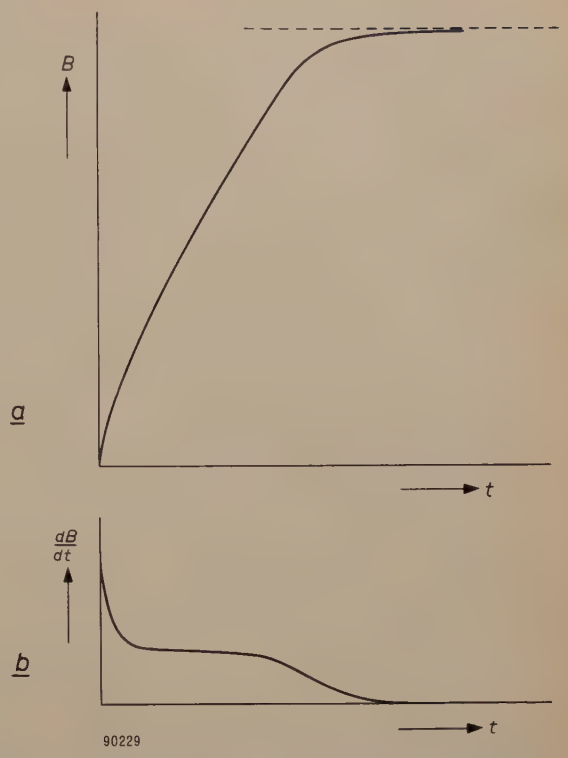

Fig. 15. *a*) The curve of fig. 14*c*, replotted with t as abscissa. *b*) Form of dB/dt as a function of t, derived from (*a*).

rent from that which applies in a slow reversal (normal hysteresis loop H_{st} in fig. 13). In the latter case the change of magnetization at each instant is, as a rule, strictly localized, whereas in a rapid reversal the magnetization at a given instant is changing at every point [2]), so that a smaller field than H_{st} is sufficient in this case, viz. H'; see *fig. 16*.

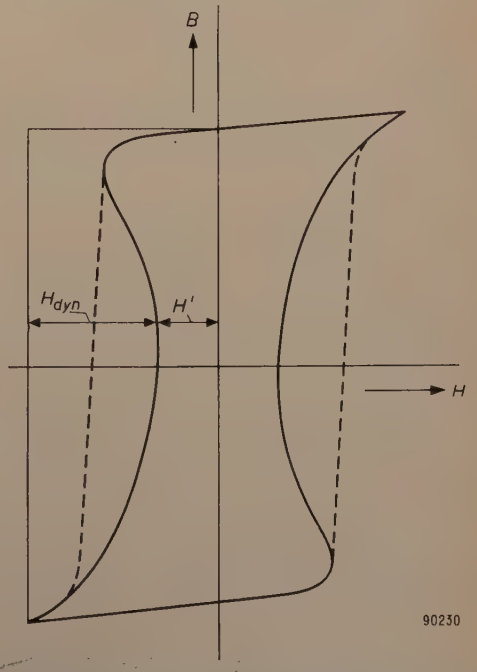

Fig. 16. Illustration of the attempt to explain the second peak in the voltage pulse, assuming that $H_{dyn} = H - H'$, and $H' < H_{st}$.

Wall displacements and rotations

We shall now endeavour to go deeper into the effects observed by taking into account the microscopic state of magnetization. We consider the Weiss domains into which a ferromagnetic material is divided and within which the elementary spins [6]) are already in parallel alignment in the non-magnetic state, though being differently orientated in different domains. The direction of magnetization in such domains is usually one of a number of preferred directions with respect to the crystal lattice (see footnote [6])). These domains are separated by relatively very thin "walls", i.e. transition boundaries, in which the magnetization passes from one direction into another. When, now, a ferromagnetic structure of this kind is magnetized by a magnetic field H, the domains in which the direction of magnetization does not make too large an angle with the direction of field will grow at the expense of adjacent domains in which this angle is larger; this amounts, therefore, to a displacement of the walls, and it gives rise to a macroscopic magnetization. An example of this is given in *fig. 17* for a frequently considered type of wall known as a 180° wall, in which the spins are parallel with the wall but in opposite directions on either side.

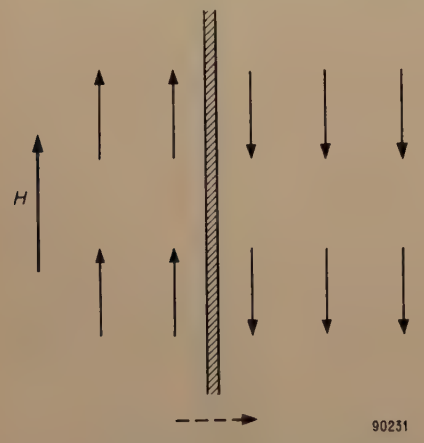

Fig. 17. Under the influence of a magnetic field H the wall of a Weiss domain (180° wall) shifts in the direction indicated by the dashed arrow.

In domains in which the magnetization is not already parallel or anti-parallel with the direction of field, the magnetization will rotate through a small angle towards H. Thus, magnetization is also produced as a result of rotation.

Wall displacements constitute by far the larger contribution in a slow reversal of magnetization in a rectangular-loop ferrite. In rapid reversals their contribution is not needed; one can imagine that the wall encounters a certain resistance during displacement and that therefore it cannot move fast enough to cover a relatively large distance in the required time. Accordingly, with the sudden application of a field H, the magnetization in the Weiss domain changes only by rotation, and now by rotation through a large angle.

In general, then, there are three possibilities as regards the change in the macroscopic magnetization: it may be caused

1) almost entirely by wall displacements,
2) almost entirely by rotations or
3) by significant contributions of both processes.

Let us return to the first sharp peak, which is almost invariably observed (fig. 4 and fig. 7). This is most probably due to rotations through a small angle. In saying this, we are really making a statement about what follows, because there is no reason why a rapidly beginning rotation should subsequently become so much slower as to give rise to the second peak already mentioned. It seems most probable, therefore, that the further course of the reversal is very largely attributable to wall displacements.

How then is the second peak to be explained? Menyuk and Goodenough [2]) postulate a cylindrical wall, the diameter of which expands at a constant rate after the sudden application of a magnetic field. The rate of wall displacement is thus assumed locally constant; the total dB/dt, however, is not constant. Since the wall covers an increasing area, dB/dt increases proportionally to the above-mentioned diameter, and the wall continues to move until it encounters another: if they are of the same type, they then both disappear. New Weiss domains do in fact frequently originate as small "spikes" [9])[10]), which subsequently spread out. The whole process is of course more complicated than described here.

It has further been observed that the second peak becomes higher and narrower at larger pulse field strengths and increasingly tends to merge with the first narrow peak (see e.g. fig. 4). There remains then one peak of relatively high voltage and very short reversal time (e.g. < 0.2 μs), which cannot be measured reliably with the apparatus described. In this case it is quite conceivable that the reversal process takes place mainly via rotations. The ferrite will be strongly magnetized by a strong field pulse of the one polarity; this means that few walls will be left in the remanent state, so that these and subsequently formed walls will have to cover a longer distance when the next pulse of opposite

[9]) J. B. Goodenough, Phys. Rev. **95**, 917-932, 1954.
[10]) L. F. Bates and D. H. Martin, Proc. Phys. Soc. A **66**, 162-166, 1953.

polarity arrives. Also, the field strength may now be sufficient to cause a reversal of magnetization without the intervention of a wall.

This can be verified by a straightforward calculation based on some very simplified assumptions.

We assume that the magnetization vector m before the field pulse makes an angle α_0 with the field direction as drawn in *fig. 18*. Upon the sudden application of field H, the vector

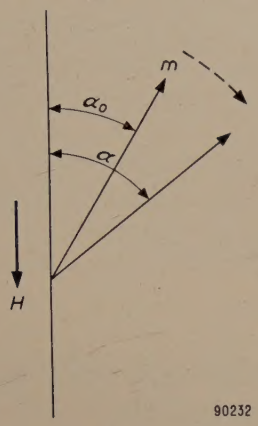

Fig. 18. A magnetic field H causes the magnetization vector m of a Weiss domain to rotate in the direction indicated by the dashed arrow.

m rotates in the sense that α becomes greater. The couple exerted by H on m is always

$$M = H\, m \sin \alpha.$$

We now assume that an opposite couple M_t arises, which is proportional to the speed of rotation of m and, of course, to m itself, since m is proportional to the volume under consideration. We thus find:

$$M_t = c\, m\, \mathrm{d}\alpha/\mathrm{d}t,$$

where the constant c is a damping constant. At every instant $M = M_t$, so that

$$\mathrm{d}\alpha/\mathrm{d}t = \frac{H}{c} \sin \alpha.$$

From this equation it follows that $\mathrm{d}B/\mathrm{d}t$ and therefore also the instantaneous voltage E of the induced pulse, is proportional to

$$\frac{H}{c} \cdot \frac{1}{\cosh^2\left(\frac{H}{c}\, t + \ln \tan \tfrac{1}{2}\alpha_0\right)}.$$

An idea of this function is given in *fig. 19*, in which the appropriate starting angle α_0 is shown at various points. The pulse form obtained is found by postulating the time $t = 0$ at α_0. Thus, at $\alpha = 90°$ there is no longer any peak.

It should be added that a smaller angle α_0 corresponds to a more rectangular hysteresis loop (higher remanence, see also I). Here again, therefore, we find that better rectangularity results in a longer switching time. In reality, α_0 is not, of course, a constant angle, but an average value around which the actual values of the angle are fairly widely spread. Moreover, the crystal anisotropy forces (see I) will also have their effect. If we take into account the fact that the magnetization m also has a mechanical momentum associated with it (gyromagnetic effect), we nevertheless obtain a very similar result for $\mathrm{d}B/\mathrm{d}t$.

Effect of mechanical stress

In the foregoing discussion of the effects of mechanical stress on ferroxcube 4A, it was shown that the stressed specimens have improved rectangularity and at the same time a longer switching time: the latter changes from 0.4 μs (no stress) to 8 μs (maximum stress), i.e. by a factor of 20 (fig. 10). This is in fact more than might be expected from the change in the form of the hysteresis loop. To explain this we must take into account the fact (see I) that in a suitable ferrite under sufficient mechanical stress there are only two preferred directions of magnetization, against 8 or 6 in unstressed ferrite. Accordingly, there are now far fewer possibilities of new Weiss domains being formed; moreover, the number of walls is also reduced owing to the greater anisotropy, so that the walls nevertheless formed must cover greater distances and therefore need more time to do so, the consequence being an extra increase in τ.

Temperature dependence

To conclude, we shall briefly discuss the dependence of the reversal process upon temperature. No matter which mechanism we consider, our calculations will always have to include one damping constant or another. (An example is the above-mentioned constant c.) If the reversal process can be made to take place exclusively via a certain type of wall, let us say a 180° wall [3]), we shall find for

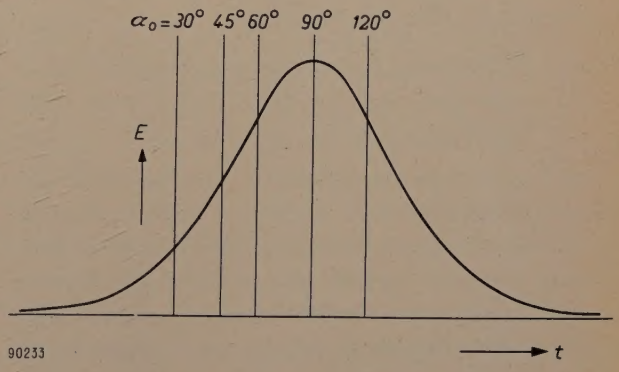

Fig. 19. The function $[\cosh^2 (Ht/c + \ln \tan \frac{1}{2}\alpha_0)]^{-1}$, representing the theoretical voltage curve if the initial value of α (i.e. at $t = 0$) is α_0. Various possible starting angles α_0 are shown.

that type of wall a certain damping constant. The question is now, what is it that mainly changes with the temperature, the damping constant itself or the manner in which the reversal process takes place? Changes in the latter with temperature are difficult to imagine in the case of rotations, but

they may well occur in the case of wall displacements. For example, a change in the crystal anisotropy and in the saturation magnetization (see I) will cause a change in the number of the walls. This effect is certainly of influence, although it appears from the article by Galt [3]) that in fact the damping constant also changes with temperature, so that the temperature dependence of the speed of reversal must be partly attributed to this.

Summary. A method is described for measuring, as a function of time, the reversal of magnetization caused by the sudden application of a magnetic field to ferrite cores with a rectangular hysteresis loop (used as "memory" elements in electronic computers). Thyratrons are used to produce the powerful current pulses needed for measurements on large ferrite rings. The variation of dB/dt during the reversal process is measured on an oscilloscope. As a function of time, dB/dt usually shows a sharp peak, followed by a second, flatter maximum, which is used for defining the "switching time". Some results are set out in graphs and tables. Beyond a certain magnetic field strength the reciprocal of the switching time is a linear function of the field strength. Separate consideration is given to the influence of external stress and temperature. The comparison of different materials as well as the study of the same material under different stresses lead to the rule: the better the squareness ratio the longer the switching time.

An attempt is made to interpret the phenomena in physical terms, the assumption being made that dB/dt is proportional to $(H-H_{st})$, where H_{st} is the value of H as a function of B, according to the statically measured hysteresis loop. In this way a reasonable explanation is given for the observed variation of dB/dt as a function of t. To explain the second peak in dB/dt an additional assumption is needed. The question is discussed in how far the reversal is effected by rotations of the magnetization vectors in the Weiss domains and wall displacements in these domains; the first sharp maximum in dB/dt is attributed to rotations, and the second peak to wall displacements. At strong fields (and hence short reversal times) there is often no second peak, in which case the entire reversal is presumably due to rotations.

ABSTRACTS OF RECENT SCIENTIFIC PUBLICATIONS BY THE STAFF OF N.V. PHILIPS' GLOEILAMPENFABRIEKEN

Reprints of these papers not marked with an asterisk * can be obtained free of charge upon application to the Philips Research Laboratory, Eindhoven, Netherlands.

2398: J. A. van Leeuwen and H. J. Oskam: Simple and sensitive leak detector (Rev. sci. Instr. **27**, 328, 1956).

Brief description of a simple and very sensitive leak detector based on the use of outgassed silica gel in conjunction with a Philips Penning gauge. The sensitivity is about 100× better than that of a palladium tube leak detector.

2399: P. Penning: Annealing of germanium supersaturated with nickel (Phys. Rev. **102**, 1414-1415, 1956).

Brief note on experiments to determine the change in density of Ni acceptor levels during the annealing of supersaturated samples of germanium. During the first periods of annealing the density of the Ni acceptor levels decreases much more rapidly than the total density of acceptor levels present in the sample.

2400: J. D. Fast: Moleculaire interpretatie van relaxatieverschijnselen (Chem. Weekblad **52**, 445-460, 1956). (Molecular interpretation of relaxation phenomena; in Dutch.)

This article is substantially the introductory address to a symposium held in Leiden in December 1955 on the subject indicated in the title. Relaxation phenomena play an important role in many varied branches of physics and chemistry, where the mechanical, dielectric or magnetic properties of the material are involved. A section dealing with the phenomenological aspects of relaxation effects, considers such concepts as loss angle, compliance (compressibility, reciprocal elastic modulus, electric and magnetic susceptibility), logarithmic decrement, relaxation and hysteresis. In a subsequent section, various actual relaxation effects are interpreted on an atomic basis. The analogy between mechanical, dielectric and magnetic relaxation is not restricted to the formal mathematical similarity: it is also often manifested in the underlying atomic mechanism. In the final section, the origins of mechanical relaxation and hysteresis in metals are considered; they are caused by movements of atoms, dislocations and domainwalls, heat transport and the shearing of crystal boundaries.

2401: O. Bosgra and H. Hoogendoorn: Enting en immuniteit bij hondeziekte en hard-pad disease van fretten (T. Diergeneeskunde **81**, 649-658, 1956). (Inoculation for immunity from distemper and hard pad in ferrets; in Dutch.)

Ferrets vaccinated with 1/50th to 1/300th dog's dose of canine distemper vaccine cultivated on embryonated hens' eggs (N.V. Philips-Roxane), prove to be completely immune against intraperitoneal infection with large doses of virulent

distemper — hard-pad virus. After vaccination with 1/900th dose, one in three ferrets proves not to be immune, the other two are. However, two ferrets vaccinated with 1/2700th dose did prove to become immune. An amount of 1/8100 dog's dose proved to be too small to immunize ferrets. From this, it can be concluded that some animals are hard to immunize with small doses of vaccine. It is therefore advisable that the distemper vaccine contains an ample quantity of active virus. After storage in a refrigerator for 9 months, it appeared that 1/200th dog's dose still gave ferrets a solid immunity. 1/600th dose did not. Vaccine containing mainly inactivated virus gives ferrets insufficient immunity when used in doses of 1/50th dog's dose. Ferrets do not show any disturbing symptoms after vaccinations, not even when vaccinated with 1 dog's dose.

2402: O. Bosgra and H. Hoogendoorn: De enting van nertsen tegen infecties met distemper- en hard-pad-virus (T. Diergeneeskunde **81**, 659-666, 1956). (Inoculation of mink against infection with distemper and hard-pad virus; in Dutch.)

Experiments are described in which mink were immunized with a living, avirulent canine distemper vaccine, cultivated in embryonated hens' eggs. Varying doses of the vaccine were administered, viz. 2, 1/5, 1/50 and 1/200 times a dog's dose, without causing adverse results. 25 days after vaccination the animals were infected; some with a virulent distemper virus, and some with virulent hard-pad virus.

The vaccinated animals proved to be completely immune. Of the other animals which were unvaccinated and infected for purposes of comparison, those infected with distemper all died showing the typical symptoms of the disease. Of those infected with hard-pad disease, some died and some recovered after having been seriously ill. It is apparent from these results together with the literature also reviewed, that canine distemper virus vaccine cultivated on embryonated hens' eggs, produces an excellent immunity in mink against both distemper and hard-pad disease.

2403: H. J. J. van Boort, N. Warmoltz and J. E. Winkelman: Human retina with a discharge flashlamp (Med. and biol. Illustration **6**, 166-170, 1956).

The article describes a quartz discharge flashlamp of maximum efficiency, by means of which a very effective light source is obtained for colour photography of the retina using the Zeiss-Nordenson camera.

The lamp is mounted end-on to the condenser lens of the apparatus and is operated at 500 volts giving an energy of 750 watt secs. The flash duration for which the light intensity is more than 50 per cent of the peak-intensity (half-peak time) is about 3.5 msec. The maximum brightness is 1.5 million stilbs and the integrated brightness 7400 stilb secs.

Some photographs of the retina taken with the flashlamp and the carbon arc are shown to demonstrate the increase in sharpness that can be obtained with the flashlamp. With smaller energy values the same lamp can be used for photographing the external eye.

2404*: J. M. Stevels and A. Kats: La représentation systémique des imperfections dans les réseaux silicium-oxygène (Verres et Réfractaires **10**, 129-134, 1956).

Translation into French of abstract No. **R 290.**

2405: A. Kats and J. M. Stevels: L'effet des rayonnements X et U.V. sur les verres silicatés, la silice fondue et le quartz crystallin, I (Verres et Réfractaires **10**, 135-150, 1956).

Translation into French of abstract No. **R 291.**

2406*: K. Teer: Uebertragungssysteme für das Farbfernsehen (Nachr. techn. Z. **9**, 196-198, 1956).

Abbreviated version of abstract No. **2381.**

2407: P. Westerhof and J. A. Keverling Buisman: Investigations on sterols, VI. The preparation of dihydrotachysterol$_2$ (Rec. trav. chim. Pays-Bas **75**, 453-462, 1956).

The preparation of dihydrotachysterol$_2$ to be used as a standard in biological experiments was studied. The best yields were obtained by reduction of tachysterol$_2$ with excess alkali metal, dissolved in liquid ammonia or suspended in a secondary amine. A laboratory method for the preparation of tachysterol$_2$ is given.

2408: F. A. Kröger: Some optical and electrical measurements on blue fluorescent ZnS-Cl single crystals (Physica **22**, 637-643, 1956).

For hexagonal ZnS-Cl single crystals, measurements of the intensity of luminescence, photoconductivity, Hall effect, thermo-luminescence and thermo-conductivity have been carried out (the latter two phenomena being the luminescence and the change in conductivity on showly warming

to room temperature after U.V. irradiation at 90° K). Analysis of the experimental results provides the following data:

a) the electron mobility at room temperature $\mu_c \approx 120$ cm^2 V^{-1} sec^{-1}; the mobility decreases with increasing temperature; *b*) the depth of traps formed by Cl^- is $\varepsilon_{Cl^-} = 0.24 \pm 0.02$ eV; *c*) the frequency of escape from Cl^- traps $s = 7 \times 10^4$ sec^{-1}; *d*) the capture cross-section of the Cl^- traps is $\sigma \approx 3 \times 10^{-21}$ cm^2; *e*) recombination levels ("killers") are situated ~ 0.7 eV below the conduction band.

2409: G. H. Jonker: Magnetic compounds with perovskite structure, IV. Conducting and non-conducting compounds (Physica **22**, 707-722, 1956).

A further experimental contribution to the knowledge of the magnetic interactions in compounds with perovskite structure is given. $LaMnO_3$ is an antiferromagnetic compound, but it is shown that it would be ferromagnetic if the cubic perovskite structure, present at high temperatures, could be preserved at low temperature. Besides the positive magnetic interaction between Mn^{3+} and Mn^{4+} ions, an interaction of the same sign is found between Mn^{3+} and Cr^{3+} ions. A survey is given of the results of this and former investigations.

2410: G. L. Meijering: Modellversuche über das Entstehen des Stapeldrahtgefüges in Wolfram (Warmfeste und Korrosionsbeständige Sinterwerkstoffe, 2, pp. 305-312, Plansee Seminar, 19-23 June 1955, Reutte, Tirol, edited by F. Benesovsky, 1956). (Model experiments on the origin of non-sag structure in tungsten; in German.)

Certain additions are known to have a marked effect on the metallographic structure of annealed tungsten wires. For example the technically important "non-sag structure" is characterized by long, rather irregular, grain boundaries making on the average a small angle with the wire axis.

Experiments were carried out with two-dimensional models consisting of 30 parallel fibres. Growth obstructions in the fibres and "leaks" in the fibre walls were distributed statistically. Thereupon "crystal growth" resulted in structures quite similar to the experimental ones. This is in accord with the view that remnants of the addition play an essential role in the realization of the non-sag structure in tungsten wires.

2411: G. L. Meijering: Erhöhung der Warmfestigkeit durch innere Oxydation von Legierungen (Warmfeste und Korrosionsbeständige Sinterwerkstoffe, 2, pp. 405-410, Plansee Seminar, 19-23 June, 1955, Reutte, Tirol, edited by F. Benesovsky, 1956). (Increase of hot-strength of alloys by internal oxidation; in German.)

Recrystallization, grain-growth and creep are strongly inhibited by internal oxidation if the oxide is formed in a very fine despersion. Coarse oxide particles have less influence on these high-temperature properties, though more than on room-temperature hardness.

2412: B. Verkerk: Autoradiography in study of surface phenomena (Nucleonics **14**, July 1956, pp. 60-64).

Notes on the technique of making surface autoradiographs of metal specimens. An example is given in which the effect of chlorine on semiconducting alumina layers is studied.

2413*: H. J. G. Meyer: Ionenschwingungsprobleme bei Uebergängen lokalisierter Elektronen in Halbleitern (Halbleiterprobleme III, edited by W. Schottky, pp. 230-260; F. Vieweg und Sohn, Brunswick 1956). (Influence of lattice vibrations on transitions of localised electrons in semi-conductors; in German).

Abbreviated version of the author's thesis, these abstracts No. **2374***.

2414: A. Claassen and L. Bastings: The photometric determination of copper by extraction as the diethyldithiocarbamate. Interferences and their elimination (Z. anal. Chem. **153**, 30-38, 1956).

Two procedures for the photometric determination of copper as the diethyldithiocarbamate complex have been investigated as to their selectivity. In the first procedure — extraction by chloroform from a citrate solution of *p*H about 8.5, containing EDTA — the following elements interfere: Hg^{II}, Ag, Au, Pt, Pd, Os, Sb^{III}, Te^{IV}, Tl^{III} and Bi. Interference by Hg^{II}, Ag, Pd, Sb^{III}, Te^{IV} and Tl^{III} can be prevented by simple measures. In the second procedure — extraction by a solution of lead diethyldithiocarbamate in chloroform from ammoniacal citrate — only Ag, Tl^{III}, Bi and Hg^{II} interfere. Interference by the first three elements can be prevented easily, leaving as the only serious interference in this method mercury in amounts above 500 μg.